Center for Environmentally Sustainable Transportation in Cold Climates

# Performance of TenCate Paving Interlayers in Asphalt Concrete Pavements

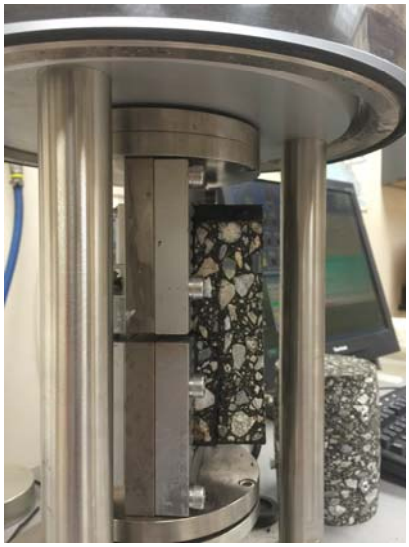


**Prepared by:**

**Jenny Liu, Ph.D., P.E.**
**Sheng Zhao, Ph.D.**
**Lin Li, Ph.D.**


**August 2017**

**Prepared for:**

**Center for Environmentally Sustainable Transportation in Cold Climates**
**University of Alaska Fairbanks**
**P.O. Box 755900**
**Fairbanks, AK 99775**

**TenCate Geosynthetics North America**
**365 South Holland Drive**
**Pendergrass, GA 30567**


**INE/AUTC 17.18**

**August 2017**

## REPORT DOCUMENTATION PAGE

Form approved OMB No.



| 1. AGENCY USE ONLY (LEAVE BLANK) | 2. REPORT DATE | 3. REPORT TYPE AND DATES COVERED |
|---|---|---|
| | 08/2017 | Final Report: 08/2015 – 08/2017 |

**4. TITLE AND SUBTITLE**
Performance of TenCate Paving Interlayers in Asphalt Concrete Pavements

**5. FUNDING NUMBERS**
INE/CESTiCC 1510

**6. AUTHOR(S)**
Jenny Liu, Sheng Zhao, and Lin Li

**7. PERFORMING ORGANIZATION NAME(S) AND ADDRESS(ES)**
Center for Environmentally Sustainable Transportation in Cold Climates
University of Alaska Fairbanks
Duckering Building Room 245
P.O. Box 755900
Fairbanks, AK 99775-5900

**8. PERFORMING ORGANIZATION REPORT NUMBER**
INE/AUTC 17.18

**9. SPONSORING/MONITORING AGENCY NAME(S) AND ADDRESS(ES)**
TenCate Geosynthetics North America
365 South Holland Drive
Pendergrass, GA 30567

Center for Environmentally Sustainable Transportation in Cold Climates
306 Tanana Loop, Duckering Building 245
Fairbanks, AK 99775-5900

**10. SPONSORING/MONITORING AGENCY REPORT NUMBER**

**11. SUPPLENMENTARY NOTES**

**12a. DISTRIBUTION / AVAILABILITY STATEMENT**
No restrictions

**12b. DISTRIBUTION CODE**

**13. ABSTRACT (Maximum 200 words)**

As a continued effort of a previously completed project entitled "Performance of TenCate Mirafi PGM-G4 Interlayer-Reinforced Asphalt Pavements in Alaska," this project evaluated two newly modified paving interlayers (TruPave and Mirapave) through overlay, dynamic modulus tests and low-temperature performance tests. A field survey was conducted to further evaluate the performance of three paving interlayers ($G^4$, G50/50, and G100/100) applied to field sections constructed in May 2013 at Milepost 148–156 Richardson Highway in Alaska. Overlay test results indicate that asphalt concrete (AC) with paving interlayers (TruPave and Mirapave) shows lower reduction in peak load, suggesting better cracking resistance. The dynamic modulus measurement of AC with paving interlayers reveals more rational results from the IDT mode test than the AMPT method due to similar stress conditions in the paving interlayer. With paving interlayers, the temperature sensitivity and cracking potential of AC material were reduced according to the results from the IDT creep test. Field survey results confirm that all sections reinforced with paving interlayers ($G^4$, G50/50, and G100/100) had better cracking resistance than the control section.

**14. KEYWORDS**
Paving interlayer, Mirapave, TruPave, reflective cracking, crack resistance

**15. NUMBER OF PAGES**
119

**16. PRICE CODE**
N/A

| 17. SECURITY CLASSIFICATION OF REPORT | 18. SECURITY CLASSIFICATION OF THIS PAGE | 19. SECURITY CLASSIFICATION OF ABSTRACT | 20. LIMITATION OF ABSTRACT |
|---|---|---|---|
| Unclassified | Unclassified | Unclassified | N/A |

# Performance of TenCate Paving Interlayers in Asphalt Concrete Pavements

***Final Report***

**Submitted to**

**TenCate Geosynthetics North America**

**by**

**Jenny Liu, Ph.D., P.E.**
**Professor**
**Department of Civil and Environmental Engineering**

**Sheng Zhao, Ph.D.**
**Research Associate**
**Center for Environmentally Sustainable Transportation in Cold Climates**

**Lin Li, Ph.D.**
**Research Associate**
**Center for Environmentally Sustainable Transportation in Cold Climates**

**August 2017**

**University of Alaska Fairbanks**
**Fairbanks, AK 99775-5900**

**Notice**

This document is disseminated under the sponsorship of the U.S. Department of Transportation in the interest of information exchange. The U.S. Government assumes no liability for the use of the information contained in this document. The U.S. Government does not endorse products or manufacturers. Trademarks or manufacturers' names appear in this report only because they are considered essential to the objective of the document.

**Quality Assurance Statement**

The Federal Highway Administration (FHWA) provides high-quality information to serve Government, industry, and the public in a manner that promotes public understanding. Standards and policies are used to ensure and maximize the quality, objectivity, utility, and integrity of its information. FHWA periodically reviews quality issues and adjusts its programs and processes to ensure continuous quality improvement.

**Author's Disclaimer**

Opinions and conclusions expressed or implied in the report are those of the author. They are not necessarily those of the Alaska DOT&PF or funding agencies.

# METRIC (SI*) CONVERSION FACTORS

## APPROXIMATE CONVERSIONS TO SI UNITS

| Symbol | When You Know | Multiply By | To Find | Symbol |
|---|---|---|---|---|
| | | **LENGTH** | | |
| in | inches | 25.4 | | mm |
| ft | feet | 0.3048 | | m |
| yd | yards | 0.914 | | m |
| mi | Miles (statute) | 1.61 | | km |
| | | **AREA** | | |
| $in^2$ | square inches | 645.2 | millimeters squared | $cm^2$ |
| $ft^2$ | square feet | 0.0929 | meters squared | $m^2$ |
| $yd^2$ | square yards | 0.836 | meters squared | $m^2$ |
| $mi^2$ | square miles | 2.59 | kilometers squared | $km^2$ |
| ac | acres | 0.4046 | hectares | ha |
| | | **MASS (weight)** | | |
| oz | Ounces (avdp) | 28.35 | grams | g |
| lb | Pounds (avdp) | 0.454 | kilograms | kg |
| T | Short tons (2000 lb) | 0.907 | megagrams | mg |
| | | **VOLUME** | | |
| fl oz | fluid ounces (US) | 29.57 | milliliters | mL |
| gal | Gallons (liq) | 3.785 | liters | liters |
| $ft^3$ | cubic feet | 0.0283 | meters cubed | $m^3$ |
| $yd^3$ | cubic yards | 0.765 | meters cubed | $m^3$ |
| | | **TEMPERATURE (exact)** | | |
| ºF | Fahrenheit temperature | 5/9 (ºF-32) | Celsius temperature | ºC |
| | | **ILLUMINATION** | | |
| fc | Foot-candles | 10.76 | lux | lx |
| fl | foot-lamberts | 3.426 | candela/$m^2$ | $cd/cm^2$ |
| | | **FORCE and PRESSURE or STRESS** | | |
| lbf | pound-force | 4.45 | newtons | N |
| psi | pound-force per square inch | 6.89 | kilopascals | kPa |

Note: Volumes greater than 1000 L shall be shown in $m^3$

These factors conform to the requirement of FHWA Order 5190.1A *SI is the symbol for the International System of Measurements

## APPROXIMATE CONVERSIONS FROM SI UNITS

| Symbol | When You Know | Multiply By | To Find | Symbol |
|---|---|---|---|---|
| | | **LENGTH** | | |
| mm | millimeters | 0.039 | inches | in |
| m | meters | 3.28 | feet | ft |
| m | meters | 1.09 | yards | yd |
| km | kilometers | 0.621 | Miles (statute) | mi |
| | | **AREA** | | |
| $mm^2$ | millimeters squared | 0.0016 | square inches | $in^2$ |
| $m^2$ | meters squared | 10.764 | square feet | $ft^2$ |
| $km^2$ | kilometers squared | 0.39 | square miles | $mi^2$ |
| ha | hectares (10,000 $m^2$) | 2.471 | acres | ac |
| | | **MASS (weight)** | | |
| g | grams | 0.0353 | Ounces (avdp) | oz |
| kg | kilograms | 2.205 | Pounds (avdp) | lb |
| mg | megagrams (1000 kg) | 1.103 | short tons | T |
| | | **VOLUME** | | |
| mL | milliliters | 0.034 | fluid ounces (US) | fl oz |
| liters | liters | 0.264 | Gallons (liq) | gal |
| $m^3$ | meters cubed | 35.315 | cubic feet | $ft^3$ |
| $m^3$ | meters cubed | 1.308 | cubic yards | $yd^3$ |
| | | **TEMPERATURE (exact)** | | |
| ºC | Celsius temperature | 9/5 ºC+32 | Fahrenheit temperature | ºF |
| | | **ILLUMINATION** | | |
| lx | lux | 0.0929 | foot-candles | fc |
| $cd/cm^2$ | candela/$m^2$ | 0.2919 | foot-lamberts | fl |
| | | **FORCE and PRESSURE or STRESS** | | |
| N | newtons | 0.225 | pound-force | lbf |
| kPa | kilopascals | 0.145 | pound-force per square inch | psi |

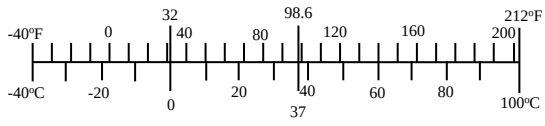

## ACKNOWLEDGMENTS

The authors wish to express their appreciation to TenCate Geosynthetics North America for its financial support. Acknowledgment of financial support and matching dollars for this project is also extended to the Center for Environmentally Sustainable Transportation in Cold Climates (CESTiCC).

## TABLE OF CONTENTS

**LIST OF FIGURES**

## LIST OF TABLES

## EXECUTIVE SUMMARY

This study complements a project completed 2 years ago (Li et al. 2014). In the previous study, the performance of several paving interlayers (i.e., G50/50, G100/100, and $G^4$) in asphalt concrete (AC) pavements was evaluated through laboratory tests and finite element method simulation. Several field experimental sections, including AC pavements reinforced with different paving interlayers, as well as a control section, were constructed on the Richardson Highway in Alaska. The performance of the pavement reinforced with these paving interlayers was evaluated during yearly surveys performed in 2013 and 2014, after field construction in July 2013. Field surveys were performed continually to further evaluate the performance of the pavement reinforced with these paving interlayers.

TenCate Geosynthetics recently modified two products, Mirapave and TruPave, by adding a release liner with high-temperature adhesive that withstands temperatures of over 400°F. The newly developed products were designed for placing over a crack only with/without overlay paved above, which might make it unnecessary to put an interlayer over the entire existing roadway to improve cracking resistance. In the current project, the overlay test, dynamic modulus tests (using an Asphalt Mixture Performance Tester [AMPT] and a dynamic modulus test in indirect tension [IDT] mode), and low-temperature performance (IDT creep) tests were performed to verify the feasibility of using these two products for crack mitigation in pavement structure used in Alaska.

The overlay test was conducted at 25°C on AC reinforced with two sizes (the entire interlayer and an interlayer strip) of TruPave or Mirapave and control AC specimens. According to the mechanism of overlay testing, a lower reduction percentage of the peak load is more desirable in terms of reflective cracking resistance. As for the peak load reduction percentage, AC specimens reinforced with two paving interlayers (Mirapave and TruPave) showed the following decreasing order: samples with an entire layer of TruPave material, control samples, samples with a TruPave interlayer strip, samples with a Mirapave interlayer strip, and samples with an entire Mirapave interlayer. The mixtures with an entire interlayer or interlayer strip generally performed better in crack resistance. Note that TruPave was adhesive on one side only. During testing, the overlay test setup may have amplified bonding weakness between the entire TruPave layer and the AC, causing early failure. More should be done to verify this finding.

Using the AMPT, the dynamic modulus test was conducted on AC reinforced with an entire layer of TruPave or Mirapave and control AC specimens at different temperature conditions (4°C, 21°C, 37°C, and 54°C) with six loading frequencies (0.1, 0.5, 1.0, 5, 10, and 25 Hz). The measured dynamic modulus (|E*|) of the control specimens is remarkably higher than the mixes with paving interlayers. The measured |E*| of AC with the paving interlayers Mirapave and TruPave was extremely low due to the inclusion of the paving interlayer and its low stiffness. Besides this, the paving interlayer was under compression rather than tension, which is different from the stress state that the fabric would experience in the field. As a result, reinforcement of the paving interlayer is not reflected by this test

Since the |E*| can also be measured in IDT mode, with the paving interlayer under tension (indirect), which is more consistent with field stress conditions, the |E*| test in IDT mode was performed at seven temperatures (-30°C, -20°C, -10°C, 0°C, 10°C, 20°C, and 30°C) with six frequencies (0.01, 0.05, 0.1, 0.5, 1, and 5 Hz). The obtained master curves of the control mixture tested using two methods (AMPT and IDT mode) were very close, which verified the rationality of the dynamic modulus measurement in IDT mode. The master curve of the TruPave and Mirapave mixtures was nearly the same or slightly higher than that of the control mixture, which was different from the |E*| results using the AMPT. According to the results presented in this study, for AC with paving interlayers (i.e., Mirapave and TruPave), the dynamic modulus measurement in IDT mode is preferable to the AMPT method.

The IDT creep test was performed at four temperatures (-30°C, -20°C, -10°C, and 20°C) on a cylindrical specimen with and without an entire paving interlayer (i.e., Mirapave and TruPave) to assess low-temperature performance. Test results revealed that the creep compliances, which were related to the viscoelastic behavior of AC, were significantly influenced by the testing temperature. When the temperature decreased from 20°C to -10°C, the creep compliance of AC with/without paving interlayers dramatically decreased. At the low temperature end (-30°C), the creep compliance of mixtures with paving interlayers was very close to that of control mixtures. As a result, the inclusion of paving interlayers in the pavement structure did not compromise the pavement performance in low-temperature cracking resistance. Also, note that the creep compliance variation of the control group was more dramatic than that of the AC with paving

interlayers. Adding a paving interlayer to the AC could reduce the temperature sensitivity of the material.

The IDT creep test results also show that the creep strain of the AC with paving interlayers could be higher or lower than that of the control groups at different temperatures. That is, the paving interlayer may/may not contribute to carrying the tensile load before AC cracks. However, when the AC layer cracks, the paving interlayer is expected to provide extra resistance to the widening of the crack due to the higher tensile strength it can carry. This crack control capability, which cannot be revealed by the IDT creep test, will be explored in future research.

In addition to the laboratory tests, yearly surveys were performed on the field sections reinforced with paving interlayers (i.e., G50/50, G100/100, and $G^4$) after construction in 2013. Four years of surveying and monitoring have shown that all test sections performed better than the control section, which indicates that placement of paving interlayers (i.e., G50/50, G100/100, and $G^4$) would benefit pavement performance. Among the sections with paving interlayers built in, the G100/100 reinforced pavement (left lane) showed the best performance, followed by the G50/50 reinforced section (left lane), then the $G^4$ section (right lane). Continued monitoring of the test sections and more detailed description of pavement distress is recommended to learn how pavement sections with paving interlayers progress with time. Having a few more years of data would provide a much clearer projection of the utility of paving interlayers in cold regions.

# CHAPTER 1 – INTRODUCTION

## Problem Statement

Paving interlayers have been used in asphalt overlays in a variety of design and construction situations for more than three decades. In a previously completed project at the University of Alaska Fairbanks (Li et al. 2014), several types of paving interlayers provided by TenCate Geosynthetics were used to explore the performance of paving interlayer-reinforced asphalt concrete (AC) pavements in Alaska. Laboratory testing and finite element method (FEM) simulation identified a number of engineering benefits of using paving interlayers in AC pavements. Further, preliminary field evaluation of test sections reinforced with paving interlayers showed better performance than the control section. However, there is concern over whether interlayers perform well continuously over time. More years of field monitoring and evaluation are recommended to further validate findings from the previous study and evaluate overall AC pavement performance in the field.

The research team continues to explore the potential of paving interlayers for AC pavement preservation and repair. Recently, two paving interlayers, Mirapave and TruPave (i.e., PGM30), were modified by adding a release liner with a high-temperature adhesive that withstands temperatures of over 400°F. The newly developed products were designed for placing over a crack only with/without overlay paved above, which might make it unnecessary to put an interlayer over

the entire existing roadway to improve cracking resistance. Laboratory evaluation is needed to verify the feasibility of using these two products for crack mitigation on roadway surfaces.

## Background

Paving interlayers have been used in AC overlays since the 1980s, and the inclusion of a paving interlayer system significantly improves the performance of AC overlays. In cold regions such as Alaska and other northern states, AC overlays are more prone to thermal cracking due to extreme climates. A previously completed study (Li et al. 2014) investigated how paving interlayers function in AC pavements in cold regions. Several types of paving interlayers including two types of bi-axial interlayers (G50/50 and G100/100) and one newly developed multi-axial reinforced paving composite ($G^4$) were used. The study completed two phases: laboratory index testing (Phase I) and field performance evaluation (Phase II). Phase I focused on laboratory evaluation of engineering properties of paving interlayer-reinforced asphalt pavement structure such as asphalt retention, grab strength, shear strength, permeability, and indirect tension tests. The results identified performance improvement of AC due to the reinforcement of all paving interlayers. Adding paving interlayer could increase pavement structure stiffness, greatly reduce permeability, and provide good resistance to low-temperature cracking and fatigue cracking. Pavement structural analysis using BISAR and Alaska Flexible Pavement Design programs (AKFPD 2004) and FEM analysis using ABAQUS were conducted. The pavement structural analyses were in agreement that using interlayer could improve fatigue

crack resistance and extend service life. The three-yarn bi-axial interlayer showed the best reinforcement potential for fatigue crack resistance, followed by the multi-axial interlayer and the two-yarn bi-axial interlayer. The FEM analysis indicated that the multi-axial interlayer could improve stress distribution more effectively than the bi-axial interlayer, as reflected by much lower maximum tensile strain on the bottom of the AC layer.

In Phase II – Field Performance Evaluation – field test sections were established in summer 2013, and pavement condition evaluation and surveys were conducted four times: in August and October 2013 and May and October 2014. No cracks were observed during two surveys in 2013. However, cracks occurred in test sections after one winter, though all sections with interlayers had fewer and less severe cracks than the control section. As field evaluation was implemented at the early stage of the pavement construction, further monitoring of field test sections was recommended to give a clearer projection of the utility of the paving interlayers in cold regions.

Recently, TenCate Geosynthetics modified two products, Mirapave and TruPave, by adding a release liner with a high temperature adhesive that would withstand temperatures over 400°F. The newly developed products were designed to be placed over a crack only with/without overlay paved above, which might make it not necessary to put an interlayer over the entire existing roadway to improve the cracking resistance. Laboratory evaluation is needed to verify the feasibility of using these two products for crack mitigation for roadway surfaces.

## Objectives

The objectives of this research were (1) to further evaluate the performance of paving interlayer-reinforced AC pavements in Alaska through three more years of field monitoring; and (2) to investigate through laboratory tests the effects of modified Mirapave and TruPave on mitigating cracking distress in roadways.

## Research Methodology

The following major tasks were accomplished to achieve the objectives of this study:

- Task 1: Continued Monitoring of Paving Interlayer Test Sections
- Task 2: Laboratory Evaluation of Modified TruPave and Mirapave for Pavement Crack Mitigation
- Task 3: Data Collection and Analyses
- Task 4: Draft of Report and Recommendations

### *Task 1: Continued Monitoring of Paving Interlayer Test Sections*

In Task 1, field trips were scheduled for the research team to continue pavement evaluation and surveys for all test sections through the project's duration. The research team identified and recorded observed pavement distress. Field examination of roadway sections included subjective descriptions and appropriate measurements (crack width, crack depth, crack spacing, and photos) according to the Distress Identification Manual for Long-term Pavement Performance (LTPP). Other information such as local climate, traffic history/pavement age, pavement structure type,

pavement management data, etc., was collected from records in the Alaska Department of Transportation and Public Facilities (ADOT&PF) Maintenance and Operation (M&O) and Design sections.

### *Task 2: Laboratory Evaluation of Modified TruPave and Mirapave for Pavement Crack Mitigation*

Following discussions between the research team and representatives from TenCate Geosynthetics, different laboratory tests were conducted to accomplish Task 2 including (1) an overlay test based on an AMPT kit; (2) dynamic modulus (|E*|) in IDT mode; (3) dynamic modulus test using an AMPT; and (4) IDT creep tests. Testing samples were produced from three groups: laboratory produced AC as control material, AC reinforced with TruPave, and AC reinforced with Mirapave.

The overlay test was conducted following the procedures according to the Texas overlay test (Zhou and Scullion 2005). The paving interlayers (TruPave or Mirapave) were placed inside the sample before the testing. When testing began, cracks started forming from the center of the bottom of the sample, and then propagated to the area where paving interlayers were placed.

The crack failure modes of samples with and without TruPave and Mirapave were observed under monotonic tension loading, in order to reveal how these paving interlayers mitigate and control the growth of cracks. Repeated tension loading was exerted to show the potential improvement using paving interlayers in fatigue cracking resistance of the AC samples.

The basic setup for the IDT test was the same as with regular IDT tests, except that a sample of two layers was used to evaluate the effects of the paving interlayers (TruPave or Mirapave) on the cracking resistance of the sample with crack (notch) existing on one layer. The testing procedures followed AASHTO T-322 (2008). In addition, the temperature chamber allowed the IDT tests to evaluate cracking performance of the patched samples at low temperatures.

The |E*| was measured by using an AMPT in accordance with AASHTO TP-79 (2008) to evaluate how the paving interlayers (Mirapave or TruPave) affect the overall performance of the sample. In addition, a dynamic modulus test in IDT mode was conducted. Three groups of samples were made for each patching material: a control group, an entire interlayer group, and an interlayer strip group.

***Task 3: Data Collection and Analyses***

In Task 3, field performance information from all test sections through the duration of Task 1 was collected. Survey results were statistically analyzed. Results served as complementary work to the results obtained from the previous project.

Compilation and analyses of laboratory data from Task 2 were performed under this task as well. Based on data analysis and interpretation, the performance of AC with the modified products and the performance of samples with paving interlayers from the previous project were compared.

### *Task 4: Draft of Report and Recommendations*

In Task 4, a final report that included two parts was produced. Part 1 is a description of the laboratory testing methods used, test procedures and results, and findings and suggestions for further study. Part 2 is the long-term performance monitoring data from periodical pavement condition evaluation and surveys through the project duration, and recommendations for use of interlayers in future Alaska pavement projects.

# CHAPTER 2 – EXPERIMENTAL DETAILS

## Materials

By adding a release liner with a high temperature adhesive that can withstand temperatures of over 400°F, TenCate Geosynthetics modified two interlayers—Mirapave and TruPave—for reflective thermal crack mitigation in AC pavement (see Figure 2.1). TenCate Mirapave nonwoven asphalt overlay fabric forms a membrane that minimizes surface water penetration of pavement systems and provides a stress relief interlayer that inhibits the propagation of reflective cracks. The TruPave engineered paving mat is a nonwoven pavement interlayer composed of high-strength fiberglass and polyester fibers conforming to ASTM D7239 (ASTM D7239 2004). TruPave is designed with low elongation and high strength to reinforce pavement sections and retard reflective cracking in overlay applications. The newly developed products provide the potential to patch existing cracks without adding an entire interlayer.

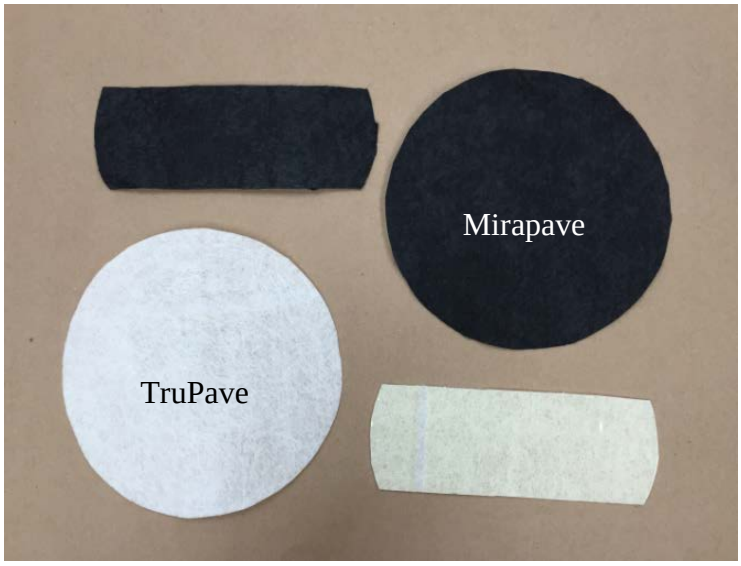


**Figure 2.1** TruPave and Mirapave paving interlayers

The performance of two paving interlayers modified for crack mitigation was evaluated. The hot mix asphalt (HMA) was a laboratory blended mixtures according to the job mix formula (JMF) used for the Richardson Highway North Pole Interchange paving project located in North Pole, Alaska. The JMF was designed according to the Marshall mix design method; PG 64-34 binder was used. The aggregate was collected from an AC mixing plant located at Peridot Street, Fairbanks, Alaska. The aggregate and binder used were from the same resources used in the paving project. The details of the JMF are presented in Appendix A.

**Specimen Preparation**

Overlay, IDT (creep test), and dynamic modulus tests were conducted to evaluate the performance of two paving interlayers (Mirapave and TruPave) when used in AC pavements. A Superpave gyratory compactor was used to compact the specimens for these tests. Since two interlayers were to be used in the AC, each specimen, including the control specimens, was compacted in two layers (i.e., 3 gyrations for the first layer and 7 gyrations for the second layer) to facilitate the placement of the fabric as schematically shown in Figure 2.2. The interlayer strip group specimens were specially used for the overlay tests. Different gyration numbers (3 for the bottom layer and 7 for the top layer) were applied to achieve the same density, relatively, in two layers. For the IDT and overlay test specimens, a total weight of 4640 g of AC was used for each specimen. The specimen after compaction was approximately 120 mm in height and 150 mm in diameter. The AC used to produce the dynamic modulus specimens by an AMPT was consistent

with the previous study, *Performance of TenCate Mirafi PGM-G[4] Interlayer-Reinforced Asphalt Pavements in Alaska* (Li et al. 2014). Specimens were compacted to 170–180 mm in height and 150 mm in diameter.

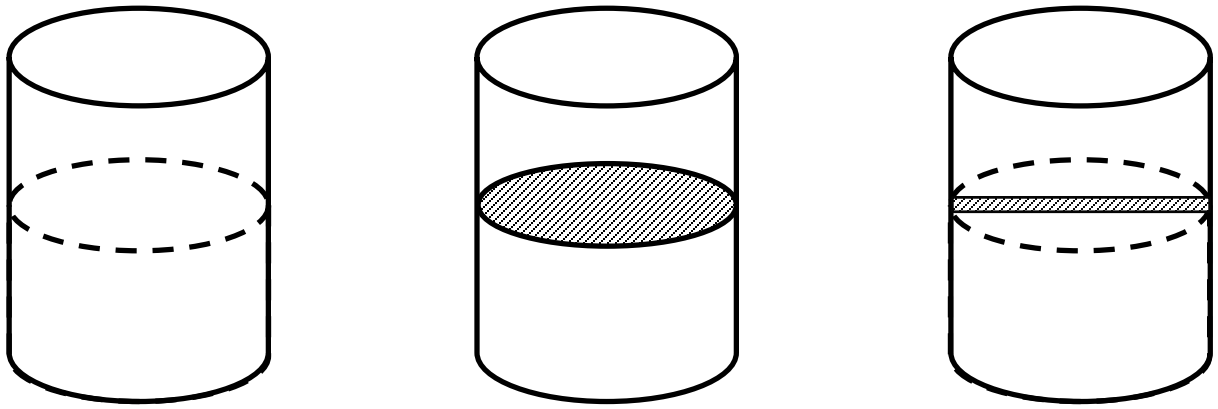

(a) (b) (c)

**Figure 2.2** Three groups of samples: (a) Control group (without patching layer); (b) Entire interlayer group for overlay, dynamic modulus, and IDT creep test; (c) Interlayer strip group for overlay test only

The detailed procedure followed three steps:

- Step 1: Load the loose mixture to the compaction mold and compact the first half of the specimen as shown in Figures 2.3a and 2.3b.
- Step 2: For the control group, do nothing. For the patching group, place the paving interlayer on top of the first half of the specimen (Figure 2.3c).
- Step 3: Load the remaining loose mixture and complete final compaction (Figures 2.3d and 2.3e).

(a) Load loose mixture

(b) Bottom layer of the specimen (inside the mold)

(c) Bottom layer of the specimen (entire interlayer or interlayer strip)

(d) Specimens compacted for the overlay, IDT tests, and dynamic modulus test in IDT mode

(e) Specimens compacted for the dynamic modulus test by the AMPT
(patching group at left, control group at right)

**Figure 2.3** Specimen compaction

Figures 2.3d and 2.3e show typical images of the compacted specimens for different tests. Three groups of samples were fabricated including the control group, patching group with Mirapave, and patching group with TruPave. When cooled to room temperature, the specimens were cut into different shapes and sizes as required for the overlay, IDT, and dynamic modulus tests.

## Material Characterization

### *Overlay Test*

The overlay test was designed by Germann and Lytton (1979) to simulate the opening and closing of joints or cracks. The overlay test is performed by applying repeated direct tension loads to a HMA specimen that is glued to two metal blocks. During testing, one block is fixed and the other slides vertically or horizontally (depends on the tester). The sliding block applies tension in a cyclic triangular waveform to a constant maximum displacement. The sliding block reaches maximum displacement and then returns to its initial position in 10 seconds. The overlay test is performed at a constant temperature of 25 ± 0.5°C. This test method measures the number of cycles to failure. The device automatically measures and records load, displacement, and temperature every 0.1 seconds. The overlay tester is run on standard-size samples (i.e., 150 mm in length, 75 mm in width, and 38 mm in height). These specimens can be prepared from either field cores or from Superpave gyratory compactor-molded specimens. Usually, three replicates are used for the overlay test.

The overlay test was conducted following the procedures according to the Texas overlay test (Zhou and Scullion 2005). Two sizes of TruPave or Mirapave, as shown in Figure 2.1, were used. The overlay test configuration is schematically shown in Figure 2.4a for the specimens with/without patching material. When the test begins, cracks form from the center of the bottom of the sample and propagate to the area where the paving interlayer is placed. In order to reveal how these paving interlayers mitigate and control the growth of cracks, the crack failure modes of specimens with and without TruPave and Mirapave were recorded under monotonic tension loading.

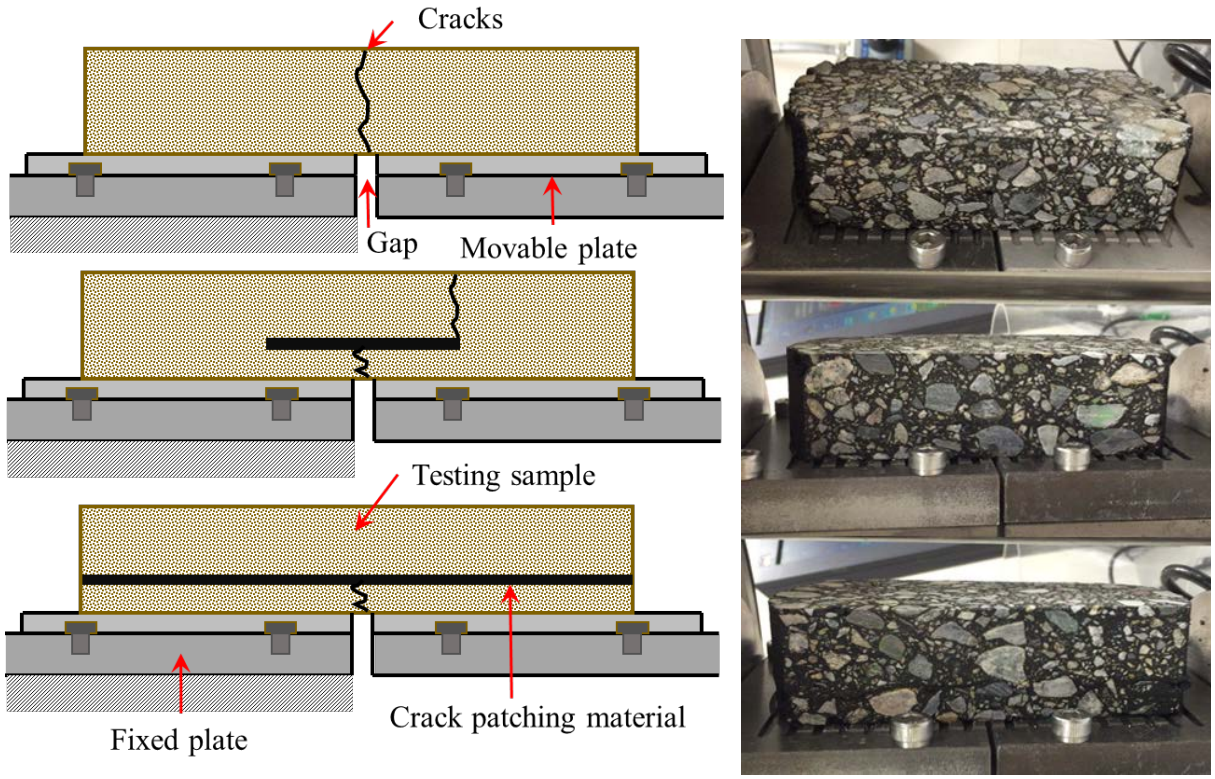


(a) Schematic of design (b) Specimen installation

**Figure 2.4** Overlay test configuration

After compaction and cooling to room temperature, the cylindrical specimens (Figure 2.3e) were cut into 150 ± 2 mm × 75 ± 0.5 mm × 38 ± 0.5 mm core specimens. The coring procedure was as follows:

1. Cut the specimens perpendicular to the top surface, trim the sides to produce specimens 76 ± 0.5 mm wide (Figure 2.5a). Discard cuttings.
2. Trim the top and bottom of each specimen to produce a sample with a height of 38 ± 0.5 mm (Figure 2.5b). Discard cuttings.

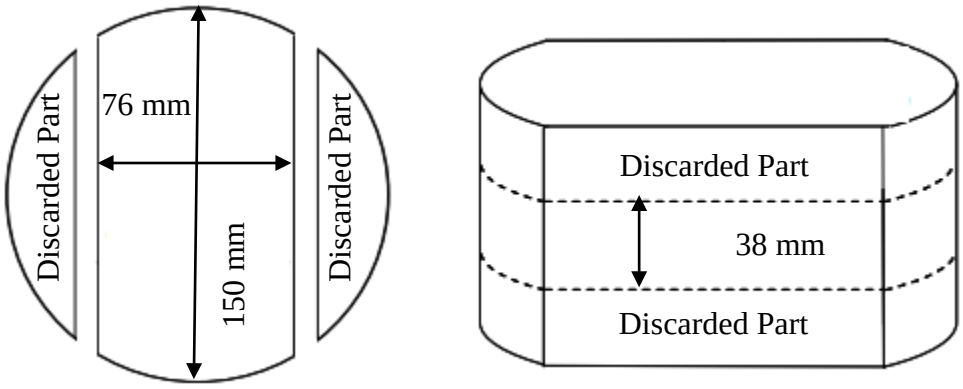


(a) (b)

**Figure 2.5** Coring specimen

After coring, the trimmed specimens were oven-dried at 40°C to constant weights. Then, using a two-part epoxy (approximately 12 g/specimen), the specimens were glued to the base plates. Note that each specimen was required to be centered and aligned parallel to the edges of the base plate. In addition, to ensure full contact with the base plates, weight was used to apply pressure to the contact surface between the specimens and the base plates. The epoxy was allowed to cure for 8 hours. Then the specimen with the base plates was installed as shown in Figure 2.4b. Figure 2.6

shows an installed specimen in the testing chamber. The temperature of the chamber was set to 25°C. The specimen was conditioned at 25°C for at least 1 hour before the overlay test.

**Figure 2.6** Overlay test setup

The test was performed in controlled-displacement mode. During testing, a cyclic load (see Figure 2.7) was applied to the moving plate to maintain a constant maximum opening displacement at 0.6 mm. To reach this displacement, one plate was fixed; the other slid vertically (see Figure 2.6.) Loading was continuously applied with the rate controlled at 10 seconds per cycle until the peak load had been reduced by at least 93% relative to the peak load at the first cycle. The test was

terminated if it had been conducted for 1000 cycles, even though the specimen had not reached 93% reduction. The output of the overlay test was the recorded load during testing, as shown in Figure 2.7.

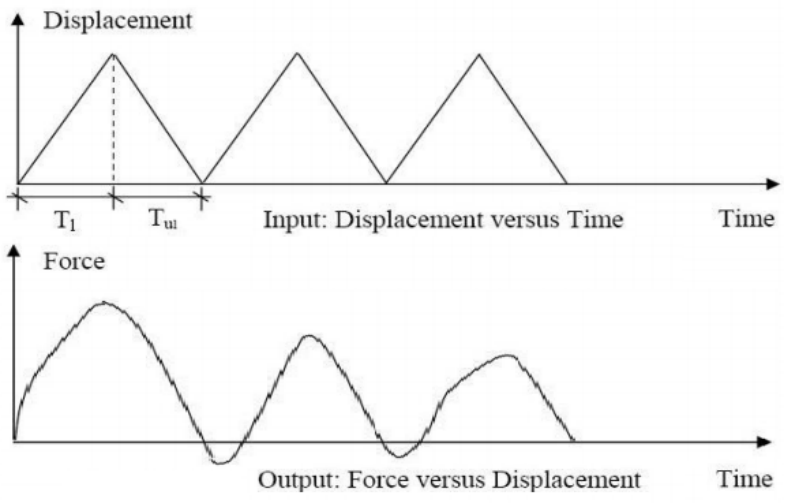


**Figure 2.7** The applied displacement and output of the overlay test

Testing results are generally interpreted by the number of loading cycles at which the sample's peak load has been reduced by 93% relative to that at the first cycle. The test ends automatically after 1000 cycles if 93% reduction is reached. In this study, the specimen with an entire layer of TruPave patching material triggered the 93% failure stop due to debonding between the fabric and the AC, as shown in Figure 2.8. Therefore, the test results were alternatively interpreted by charts depicting the change of peak load reduction percentage with the change of loading cycles. The peak load, which usually is the recorded maximum load for the first loading cycle, and the associated peak load reduction percentage for each specimen are presented in Figures 2.9a and 2.9b, respectively. The introduction of a paving layer did influence the peak load

of the specimen, and this influence was dependent on the size of the paving interlayer according to the result presented in Figure 2.9a, which was reasonable since the presence of the paving interlayer reduced load transferring to the adjacent area. Besides this, the peak load was also influenced by the property of the paving material and the associated bonding condition. With the same size of paving interlayer, the peak load of AC with Mirapave was consistently higher than the peak load of AC with a TruPave interlayer. As shown in Figure 2.9b, the sample with an entire layer of TruPave interlayer showed the highest peak load reduction percentage at the same loading cycles, followed by control samples, then the other three groups. The samples' reactions to the applied load were mostly differentiable in the first 100 cycles. Data from the first 100 cycles have been extracted and are presented in Figure 2.10. Among three groups with lower reduction percentage, samples with TruPave interlayer strip showed the highest reduction percentage, followed by samples with interlayer strip and an entire layer of Mirapave material. However, the difference within the three groups was not significant.

**Figure 2.8** Specimen debonding during overlay testing

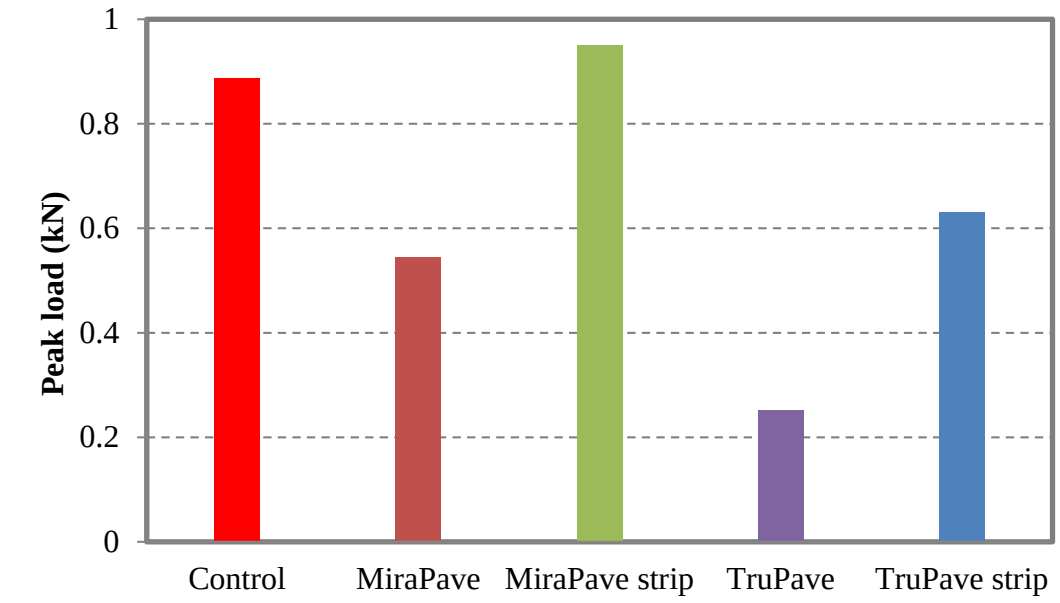


(a) Peak load

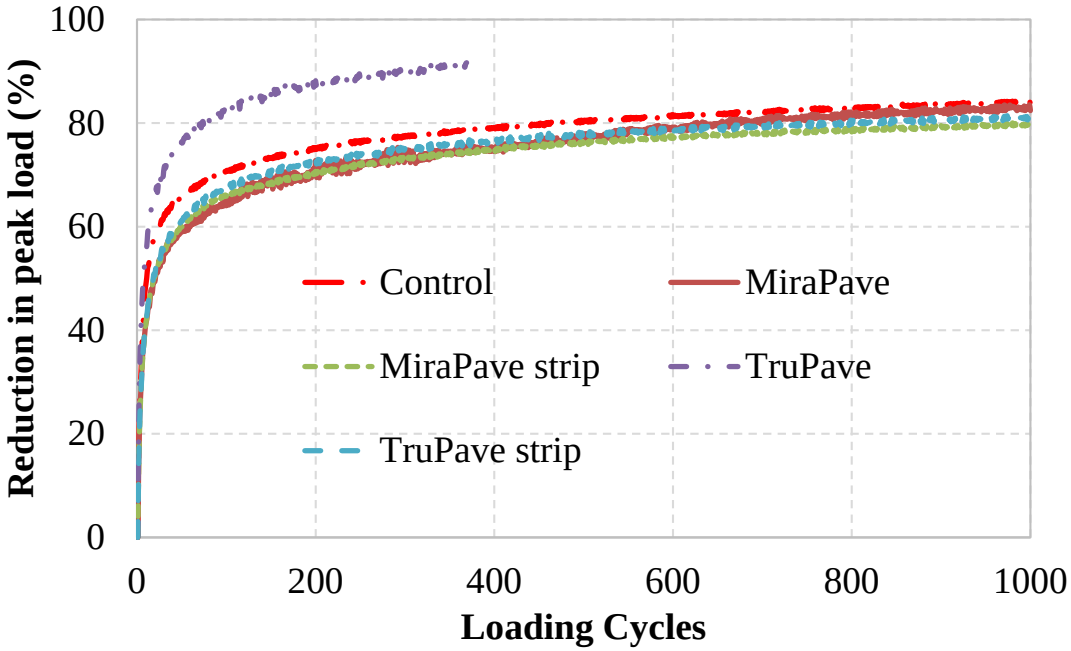


(b) Reduction in peak load

**Figure 2.9** Overlay test results for control AC and AC with paving interlayers (strip or entire layer)

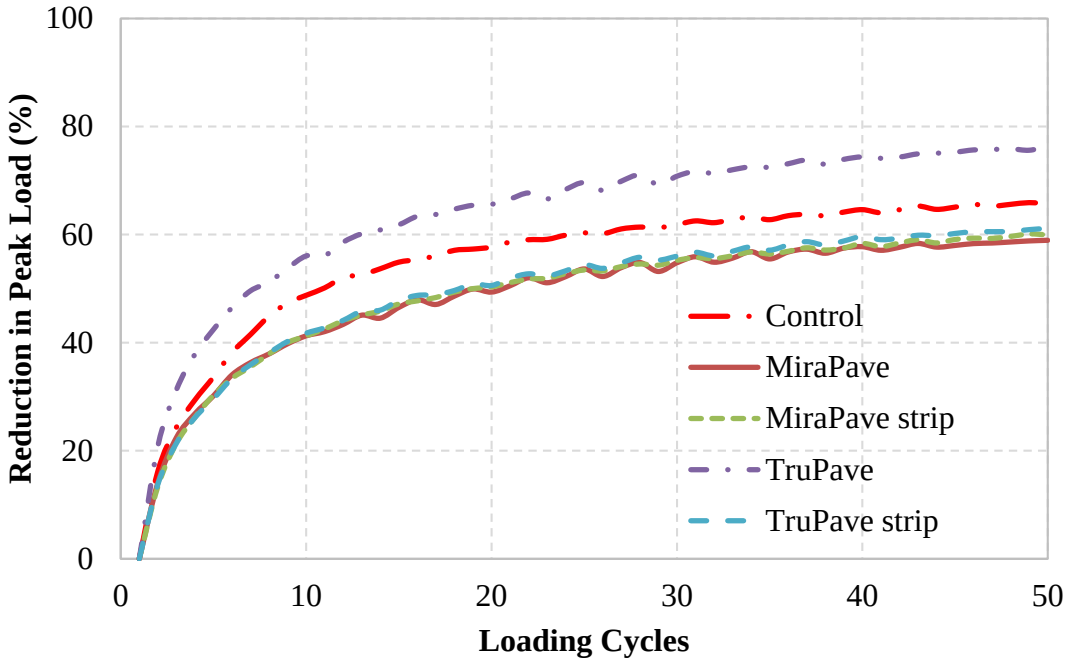


**Figure 2.10** Overlay test results for first 100 loading cycles

According to the mechanism of the overlay test, a lower reduction percentage of the peak load is more desirable in terms of reflective cracking resistance. That being said, the results displayed in Figures 2.9 and 2.10 seem supportive of using paving interlayers. As previously discussed and displayed in Figure 2.8, the early failure of samples with an entire layer of TruPave might be subject to debonding between the asphalt mixture and the TruPave interlayer. Note that TruPave is adhesive on one-side only. In this study, the adhesive side faced down when placed to simulate patching an assumable crack on top of the bottom layer. A layer of HMA was then placed on top of the non-adhesive side of the TruPave material. The two layers of samples with an entire layer of TruPave cracked first and then debonded, as shown in Figure 2.8, when subject to tensile stress. This failure of AC with an entire layer of TruPave does not necessarily mean that the

inclusion of TruPave in the pavement structure would not be beneficial in terms of crack mitigation. The stress condition in the overlay test differed from conditions in the field, where the pavement structure is normally under traffic load.

***Dynamic Modulus Test***

*Dynamic Modulus Test Using the AMPT*

The dynamic modulus (|E*|) test was measured by the AMPT in accordance with AASHTO TP-79 (2008) to evaluate how the paving interlayers (entire layer of Mirapave or TruPave) affected the overall performance of the sample. The tests were performed on cylindrical specimens cored to 100 mm in diameter and 150 mm in height (Figure 2.11). Figure 2.12 presents the AMPT testing equipment. To take into account the time-temperature dependence of |E*|, the test was performed at four temperatures (4°C, 21°C, 37°C, and 54°C) and at least six frequencies (0.1, 0.5, 1.0, 5, 10, and 25 Hz) (AASHTO TP-62 2008). The testing results are presented in Figures 2.13–2.16.

**Figure 2.11** Dynamic modulus test samples (left to right: control, Mirapave, TruPave)

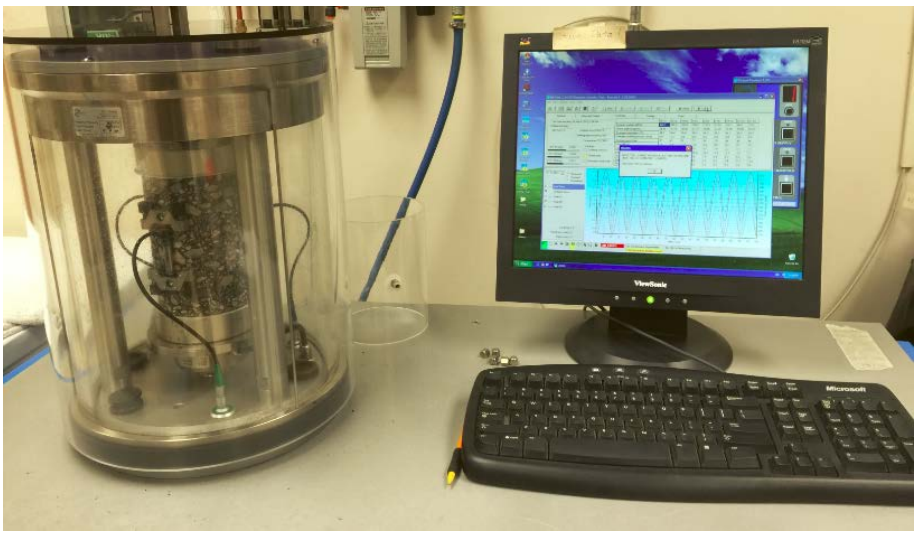

**Figure 2.12** Dynamic modulus test setup

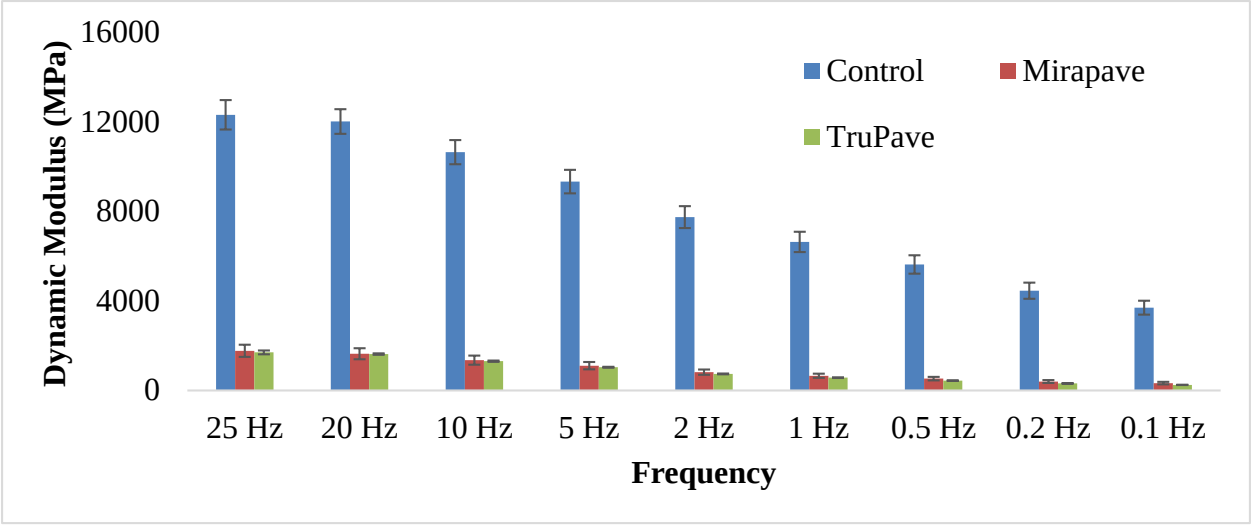


**Figure 2.13** Dynamic modulus results tested at 4°C

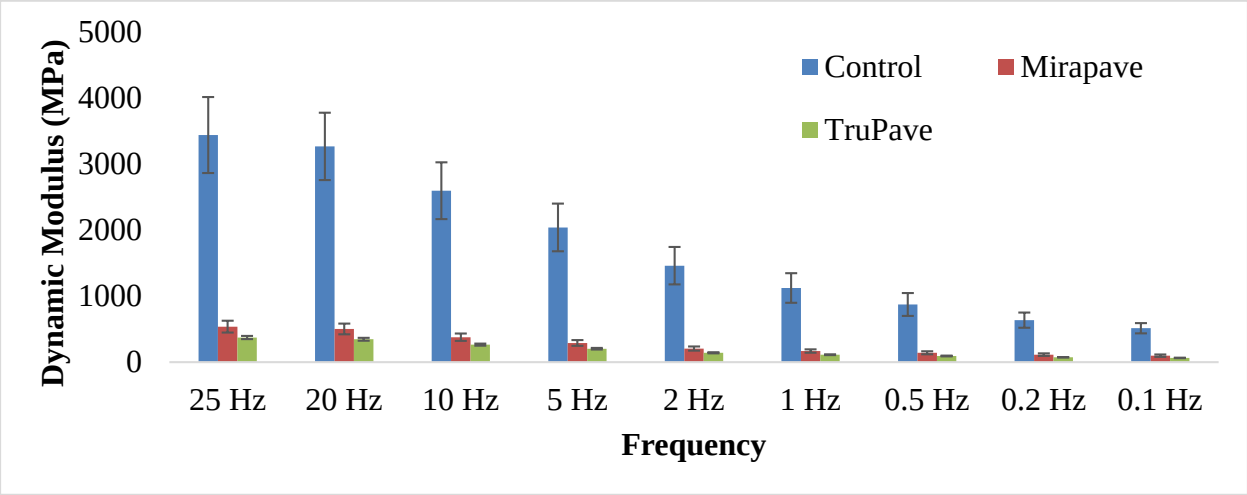


**Figure 2.14** Dynamic modulus results tested at 21°C

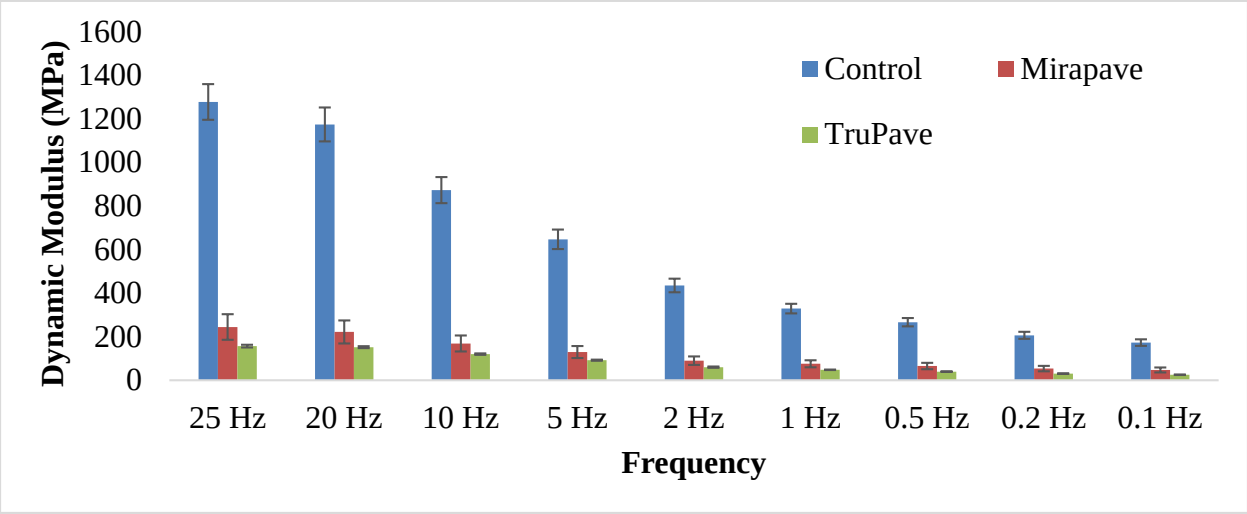


**Figure 2.15** Dynamic modulus results tested at 37°C

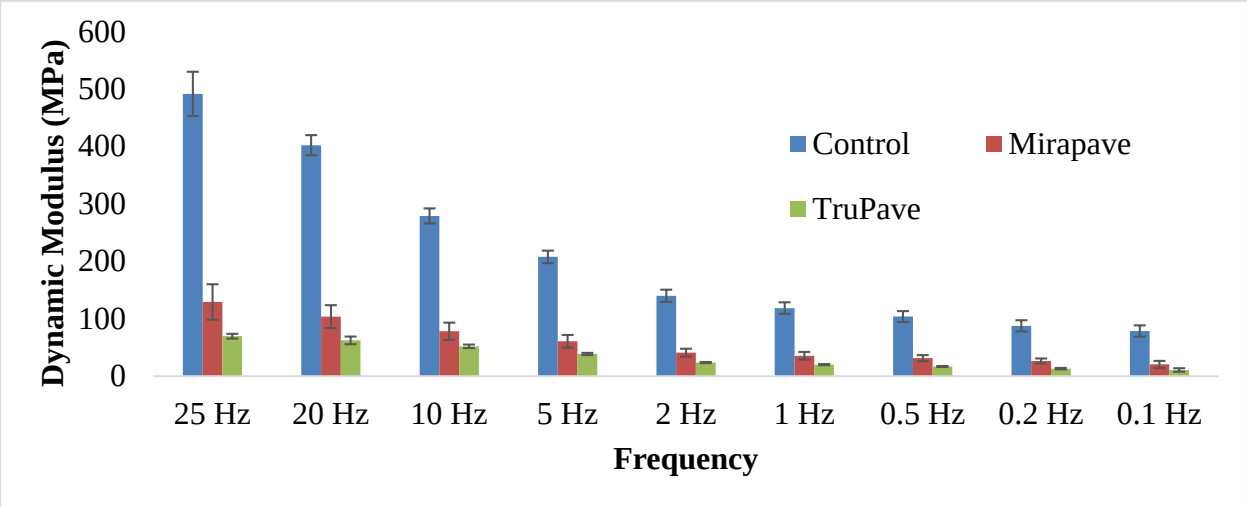


**Figure 2.16** Dynamic modulus results tested at 54°C

According to Figures 2.13 to 2.16, the measured |E*| of control specimens was remarkably higher than the mixes with paving interlayers. At low temperature levels, the measured |E*| of the Mirapave-treated specimen was nearly the same as that of the TruPave-treated specimen. However, with increasing temperature, it was found that the |E*| of the Mirapave-treated specimen rose higher than that of the TruPave-treated specimen. Using the principle of time-temperature superposition, a master curve was constructed by shifting the data at various temperatures to the reference temperature (21°C) with respect to the time until the curves merge into a single smooth function. The master curves of three groups are organized in Figure 2.17, where it can be seen that the master curves of all paving interlayer-treated specimens were substantially lower than the master curve of the control mix, indicating that interlayer-treated specimens had lower |E*|. The measured |E*|, which was extremely low, exceeded the lower limit of input for the Mechanistic

Empirical Pavement Design Guide (MEPDG) (ARA, Inc. 2000). Consequently, the pavement structure analysis could not be performed.

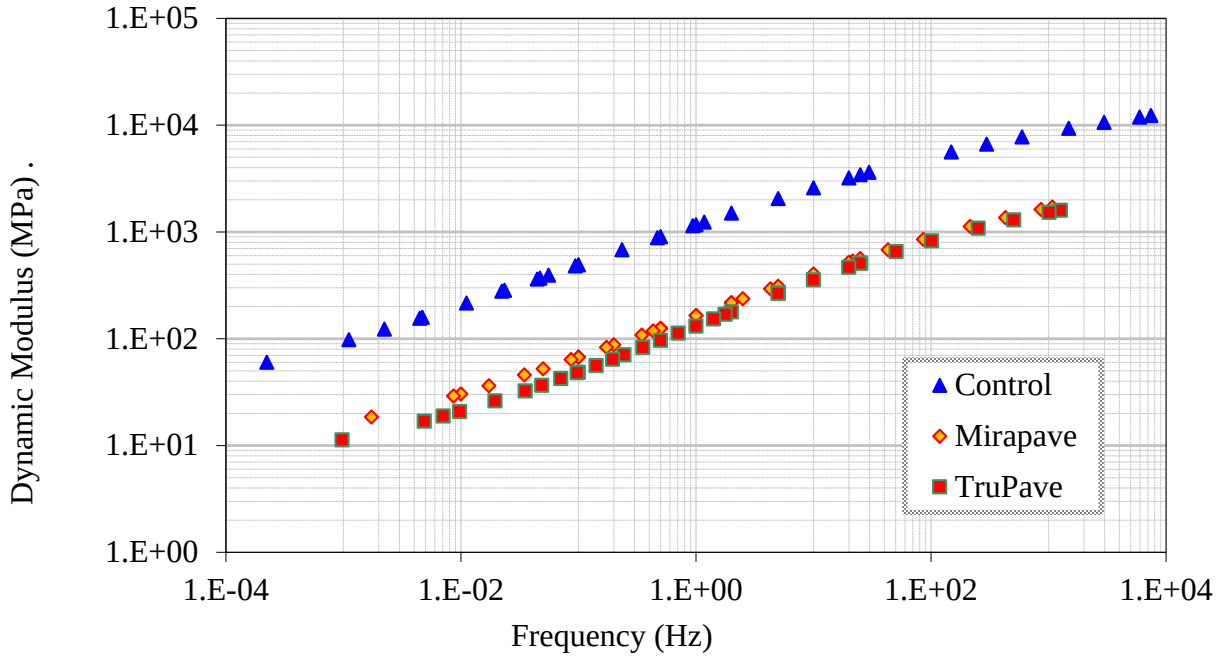


**Figure 2.17** Master curves of dynamic modulus test results using the AMPT

Since the mix part used for the specimens was the same as the mix used for the control sample, the low |E*| of the specimens with paving interlayer was attributed to the inclusion of the paving interlayer and its low stiffness. In addition, the paving interlayer was under compression rather than tension, which is different from the stress state that the fabric would experience in the field. As a result, the reinforcement of the paving interlayer could not be reflected by this test. The paving interlayer is used to improve the cracking resistance of the AC layer structure by taking advantage of its high tensile strength; thus, the measured |E*| was not representative. In addition to using the AMPT, the |E*| can be measured in IDT mode as reported by Kim et al. (2004). In the

|E*| test in IDT mode, the paving interlayer is under tension (indirect), which is more consistent with field stress conditions, so the |E*| test in IDT mode is preferable to the AMPT method of measuring |E*|.

*Dynamic Modulus Test in IDT Mode*

Besides the dynamic modulus (|E*|) test using the AMPT in accordance with AASHTO TP-79 (2008), the dynamic modulus test was performed in IDT mode according to the method proposed by Kim et al. (2004). Instead of four temperatures (4°C, 21°C, 37°C, and 54°C) and six frequencies (0.1, 0.5, 1.0, 5, 10, and 25 Hz), the AC mixtures were tested at seven temperatures (-30°C, -20 C, -10°C, 0°C, 10°C, 20°C, and 30°C) with six frequencies (0.01, 0.05, 0.1, 0.5, 1, and 5 Hz). The dynamic modulus test in indirect tension (IDT) mode was conducted to determine the dynamic modulus at different temperature and loading frequencies. The test setup for this dynamic modulus test is consistent with the setup of the conventional IDT creep test. The applied cyclic load causes the specimen to deform. At each testing temperature, normalized horizontal and vertical deformations were measured using a linear variable differential transformer (LVDT). To determine the dynamic modulus, a programmed data acquisition system was used to record the load and deformation of the specimens during testing under haversine loading.

After testing, the dynamic modulus of the tested AC was calculated using Equation 2.1, which was developed by Kim et al. (2004):

$$\left|E^*\right| = 2\frac{P_0}{\pi ad}\frac{\beta_1\gamma_2 - \beta_2\gamma_1}{\gamma_2 V_0 - \beta_2 U_0} \tag{2.1}$$

where

$E^*$ = dynamic modulus,

$P_0$ = amplitude of the applied load,

$a$ = loading strip width, m,

$d$ = thickness of specimen, m,

$V_0$ and $U_0$ = the constant amplitudes of vertical and horizontal displacements, respectively, and

$\beta_1$, $\beta_2$, $\gamma_1$, and $\gamma_2$ = coefficients calculated for different specimen diameters and gauge lengths.

Note that the last five cycles of data were analyzed and fitted according to the following functional form:

$$f(t) = l + mt + n\cos(\omega t + \phi) \tag{2.2}$$

where

$f(t)$ = load or deformation time history,

$l$, $m$, and $n$ = regression coefficients, $n$ represents the amplitude of the sinusoidal waveform,

$\phi$ = phase angle, and

$\omega$ = angular frequency.

The dynamic modulus of the tested AC was calculated from the ratio of these coefficients from load and deformation histories. Figure 2.18 presents the dynamic modulus of the mixtures tested at different temperature and loading frequencies, calculated using Equation 2.1. Based on the results presented in Figure 2.18, the master curves (reference temperature of 20°C) of mixtures with different paving interlayers (i.e., Mirapave and TruPave) as well as the control mixture were

constructed (see Figure 2.19). The master curves of the control mixture tested in two methods (AMPT and IDT mode) were very close, which verified the rationality of the dynamic modulus measurement in IDT mode. The master curves of the TruPave and Mirapave mixtures were, respectively, close to or slightly higher than the master curve of the control mixture. A comparison between the master curves based on |E*| by AMPT and IDT mode dynamic modulus tests is presented in Figure 2.19. For the mixtures with fabrics, the dynamic moduli measured by the AMPT were substantially lower than those from the IDT mode dynamic modulus measurement. As previously discussed, the major difference between the AMPT and IDT mode dynamic modulus measurement was the stress state in the paving interlayer during testing. Using the IDT mode, the stress state in the paving interlayer was consistent with the stress state in the field condition when the paving interlayer was used for reflective crack mitigation purposes. For this reason, the dynamic modulus measurement in IDT mode is preferable to the AMPT method for AC with paving interlayers.

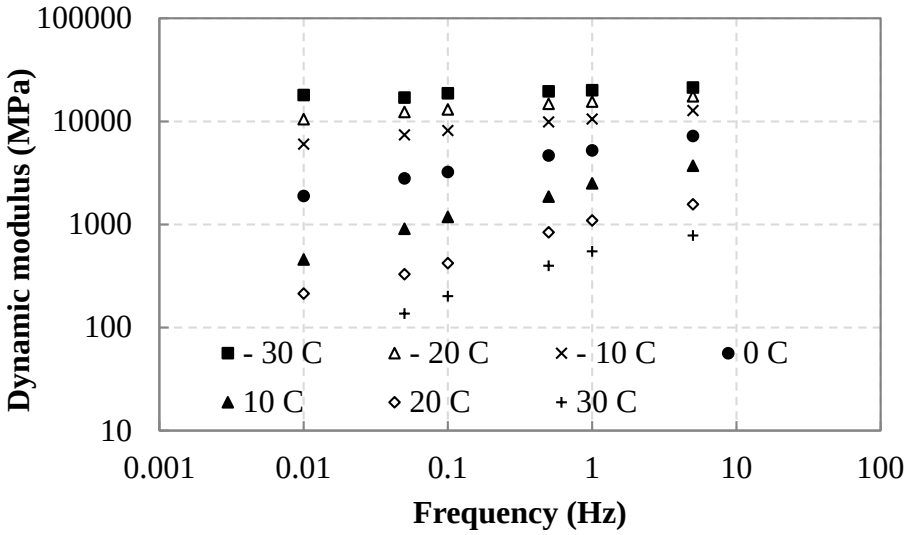


(a) Control

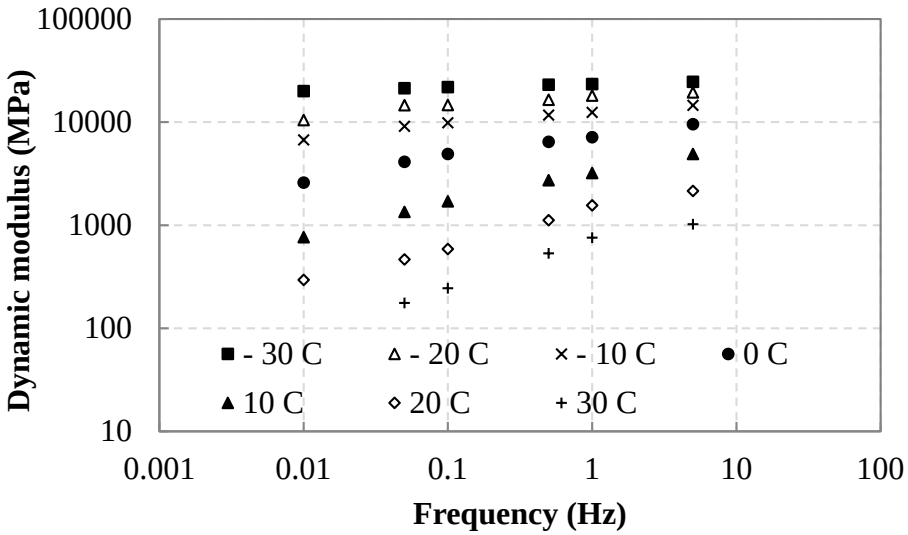


(b) Mirapave

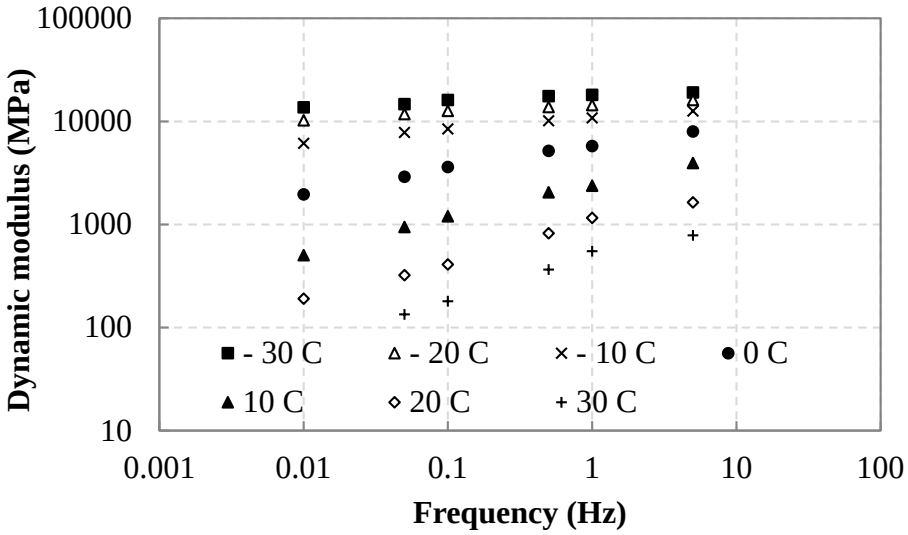


(c) TruPave

**Figure 2.18** Measured dynamic modulus in IDT mode

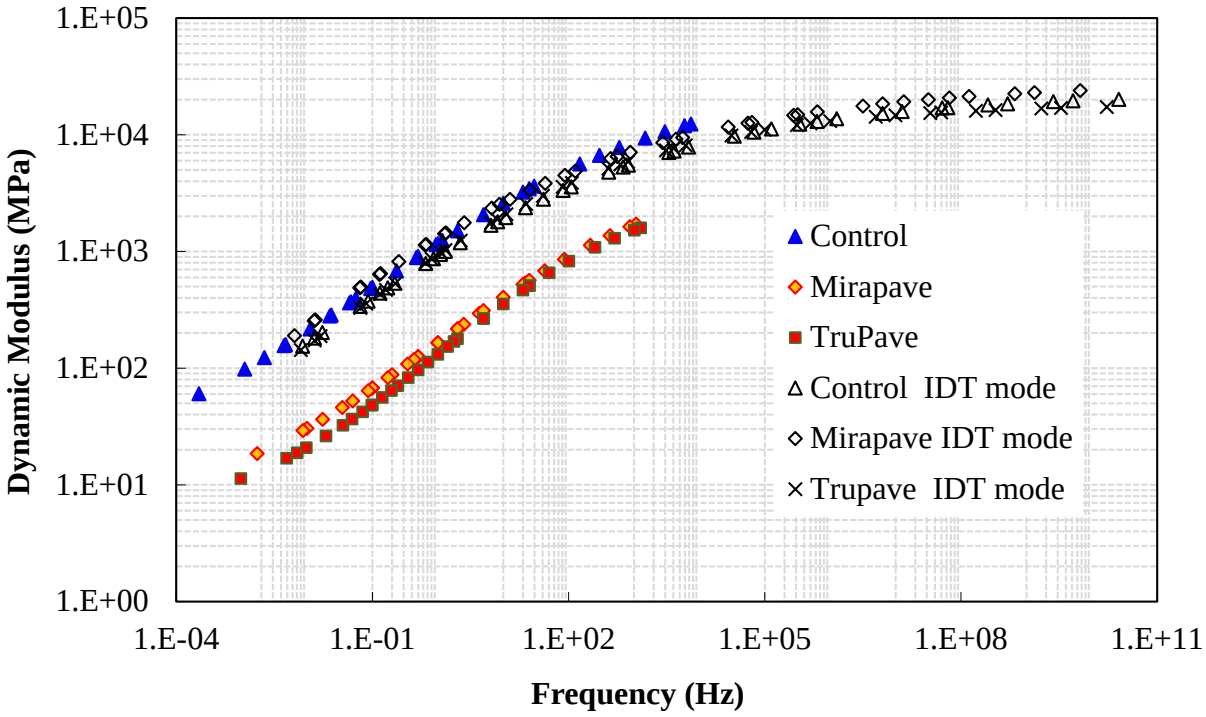


**Figure 2.19** AMPT and IDT mode dynamic modulus measurement results

***Low-Temperature Performance Test***

The IDT creep test was used to evaluate the low-temperature performance of AC with two paving interlayers (i.e., an entire layer of Mirapave and TruPave). The setup for the IDT creep test is shown in Figure 2.20. An environmental chamber, in which the temperature could be controlled, was used to condition the specimens to different target temperatures. To determine the tensile creep stiffness *S(t)* according to AASHTO specification T-322-07, a programmed data acquisition system was used to record the load and deformation of the specimens during testing.

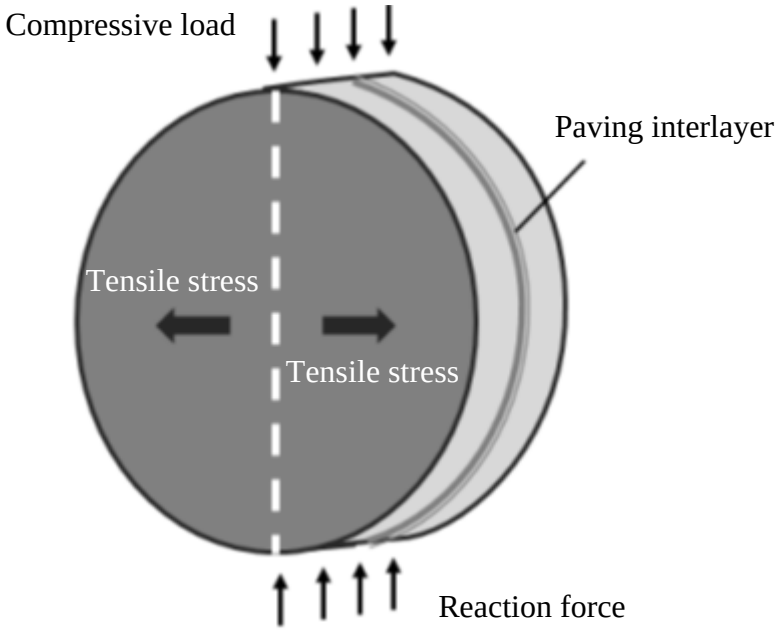


**Figure 2.20** IDT test

The IDT creep test was performed by loading the cylindrical specimen with a constant compressive load (see Figure 2.20). The applied compressive load causes the specimen to fail by splitting along the vertical direction. Specimens were approximately 50 mm in height and 150 mm in diameter. The tensile creep compliance *D(t)* of each mixture was monitored at three or four

temperatures, that is, at -30, -20, -10, and 20°C, according to the binder's low-temperature grade. At each testing temperature, normalized horizontal and vertical deformations from six specimen faces (three specimens, two faces/specimen) were measured with the LVDT (Figure 2.21).

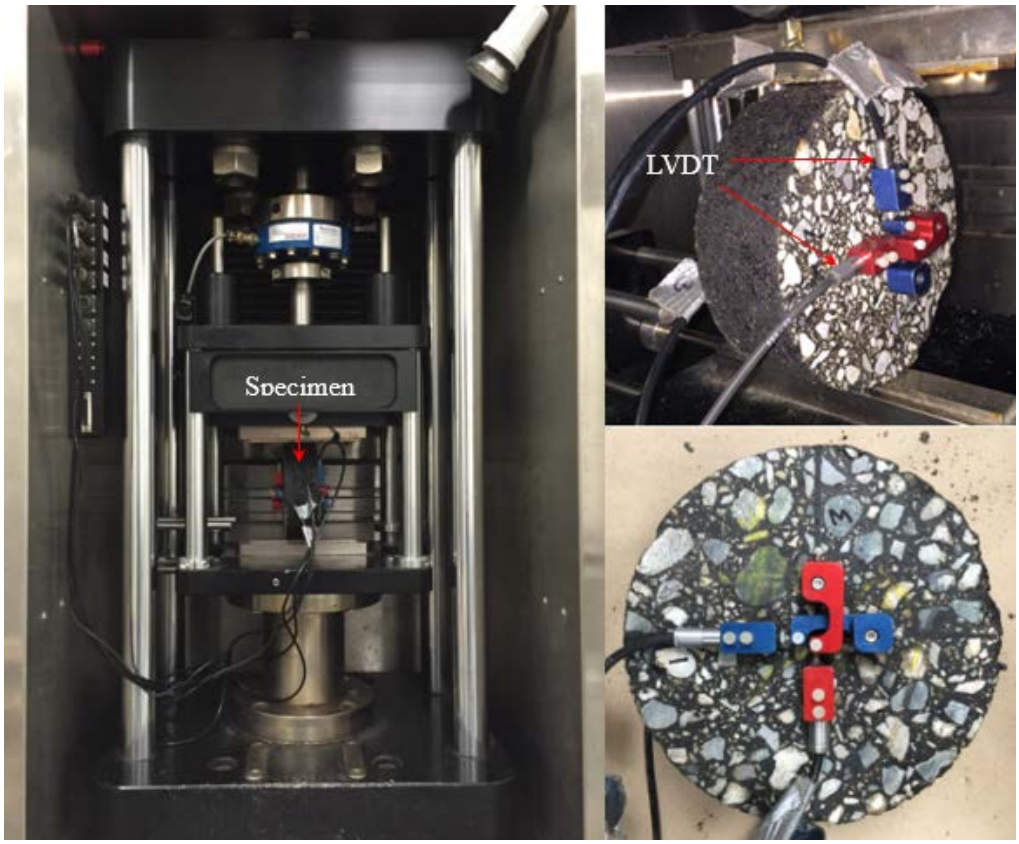


**Figure 2.21** Setup for IDT creep test

The creep compliance *D(t)* of each mixture (a viscoelastic property of HMA used in the MEPDG to calculate thermal stress at low temperatures) was tested and calculated according to Eq. 2.3:

$$D(t) = \frac{\Delta X \times D_{avg} \times b_{avg}}{P_{avg} \times GL} \times C_{cmpl} \quad (2.3)$$

where

$D(t)$ = creep compliance (kPa),

$\Delta X$ = trimmed mean of the horizontal deformations (m),

$D_{avg}$ = average specimen diameters (m),

$b_{avg}$ = average specimen thickness (m),

$P_{avg}$ = average force during the test (kN),

$GL$ = gage length (38 mm), and

$C_{cmpl}$ = creep compliance parameter at any given time, computed as

$$C_{cmpl} = 0.6354 \times \left(\frac{X}{Y}\right)^{-1} - 0.332 \quad (2.4)$$

where

$X$ = horizontal deformation, and

$Y$ = vertical deformation.

Creep stiffness $S(t)$ at the time $t$ was calculated as the inverse of the creep compliance $D(t)$:

$$S(t) = \frac{1}{D(t)} \quad (2.5)$$

After the IDT creep tests using Eqs. 2.3 and 2.4, creep compliance, which is related to the viscoelastic behavior of AC, was significantly influenced by temperature. The AC samples with/without paving interlayers at different loading temperatures were obtained and summarized (see Table 2.1). When temperature decreased from 20°C to -10°C, the creep compliance of AC with/without paving interlayers dramatically decreased. The creep compliances of the AC reinforced with TruPave were very close to or slightly lower than those of the control mixtures at different temperatures. However, the creep compliances of Mirapave-reinforced AC were lower

than those of the control AC especially at -10 and 20°C. At the low-temperature end (i.e., -30°C), the creep compliances of mixtures with paving interlayers were comparable with the control mixtures.

**Table 2.1** Summary of creep compliance (1/GPa)

| Temperature (°C) | Material | Time (s) | | | | | | |
|---|---|---|---|---|---|---|---|---|
| | | 10 | 20 | 50 | 100 | 200 | 500 | 1000 |
| 20 | Control | 8.942 | 9.973 | 13.055 | 15.415 | 18.839 | 24.090 | - |
| | Mirapave | 4.749 | 5.821 | 7.364 | 9.074 | 11.708 | 14.299 | - |
| | TruPave | 7.724 | 9.231 | 13.352 | 16.370 | 20.551 | 26.064 | - |
| -10 | Control | 0.162 | 0.191 | 0.246 | 0.327 | 0.423 | 0.575 | 0.746 |
| | Mirapave | 0.109 | 0.135 | 0.179 | 0.217 | 0.278 | 0.384 | 0.499 |
| | TruPave | 0.147 | 0.169 | 0.221 | 0.283 | 0.356 | 0.491 | 0.643 |
| -20 | Control | 0.093 | 0.103 | 0.124 | 0.146 | 0.174 | 0.219 | 0.276 |
| | Mirapave | 0.063 | 0.071 | 0.087 | 0.103 | 0.121 | 0.153 | 0.188 |
| | TruPave | 0.078 | 0.088 | 0.102 | 0.117 | 0.137 | 0.166 | 0.196 |
| -30 | Control | 0.051 | 0.055 | 0.061 | 0.068 | 0.073 | 0.081 | 0.087 |
| | Mirapave | 0.048 | 0.053 | 0.060 | 0.068 | 0.075 | 0.087 | 0.097 |
| | TruPave | 0.044 | 0.048 | 0.052 | 0.056 | 0.061 | 0.071 | 0.079 |

Usually, AC with lower creep compliance is considered more susceptible to low-temperature cracking. Since cracking due to thermal contraction only occurs at low temperatures, the creep compliance of AC with/without paving interlayers at subfreezing temperatures are plotted in Figure 2.22. At very low temperatures (i.e., -30°C), the creep compliances of mixtures with paving interlayers were close to those of the control mixtures. As a result, the inclusion of the paving interlayers in the pavement structure did not compromise pavement performance in low-temperature cracking resistance. Note that the variation of creep compliance in the control group was more dramatic than that of the mixtures with paving interlayers, as shown in Figure 2.22. In

other words, adding paving interlayer to AC could reduce the temperature sensitivity of the material, which is consistent with the research findings in the previous study (Li et al. 2014).

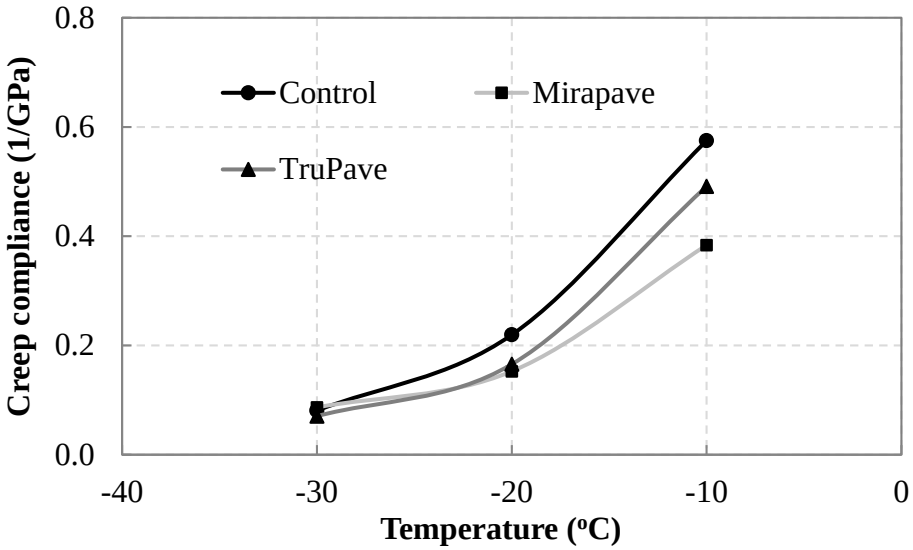


**Figure 2.22** Effect of temperature on creep compliance (500s)

Figure 2.23 shows the creep curves of horizontal tensile strain for three groups of materials at four different temperatures (20°C, -10°C, -20°C, and -30°C). It was found that the creep strain of AC with paving interlayers could be higher or lower than the creep strain of the control groups at different temperatures. The major reason for this is the differences in paving interlayers and the bonding between the AC and the paving interlayers. For example, as shown in Figure 2.23b, the creep strain of the samples with paving interlayers tested at -10°C was lower than the control sample, which is consistent with the findings presented in the previous study (Li et al. 2014). The reduction of creep compliance of interlayer-treated specimens was attributed to the applied load mostly carried by the interlayer, and the load on the HMA was reduced. In other words, the paving

interlayer was protecting the AC layer from cracking. However, the creep strain of the samples with paving interlayers tested at -30°C was higher than the creep strain of the control sample, which means the paving interlayer did not contribute in carrying tensile load in the AC. However, this finding is still considered beneficial, since AC with a higher creep rate is less prone to low-temperature cracking.

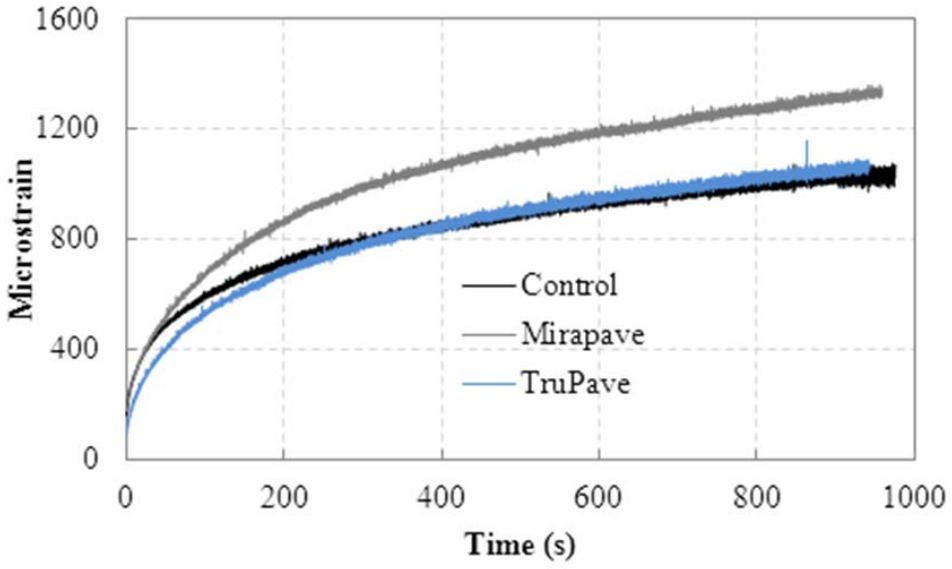


(a) 20°C, 0.15 kN vertical load

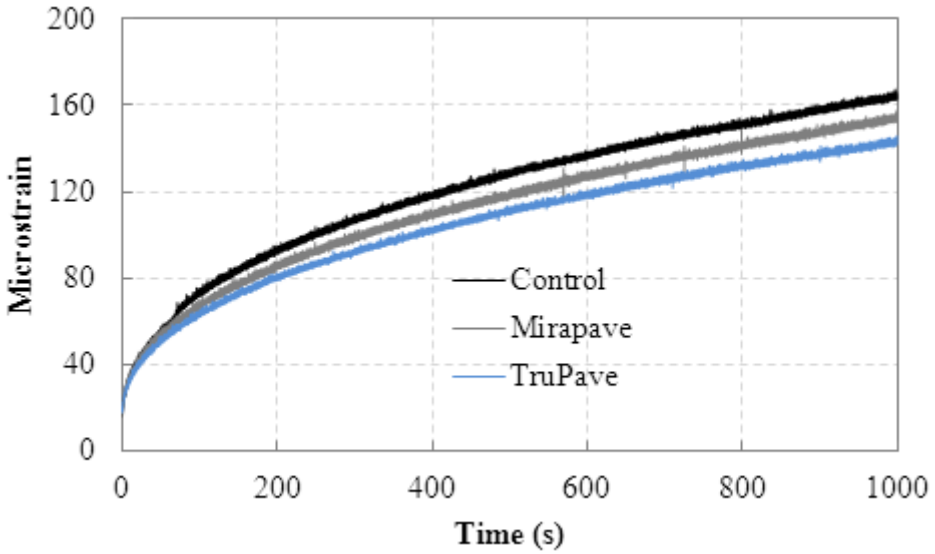


(b) -10°C, 1.5 kN vertical load

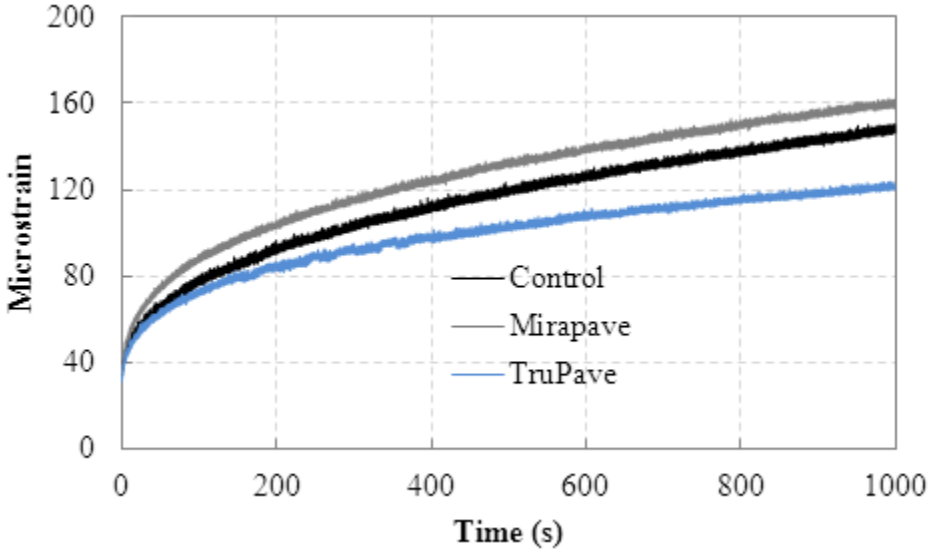


(c) -20°C, 4.4 kN vertical load

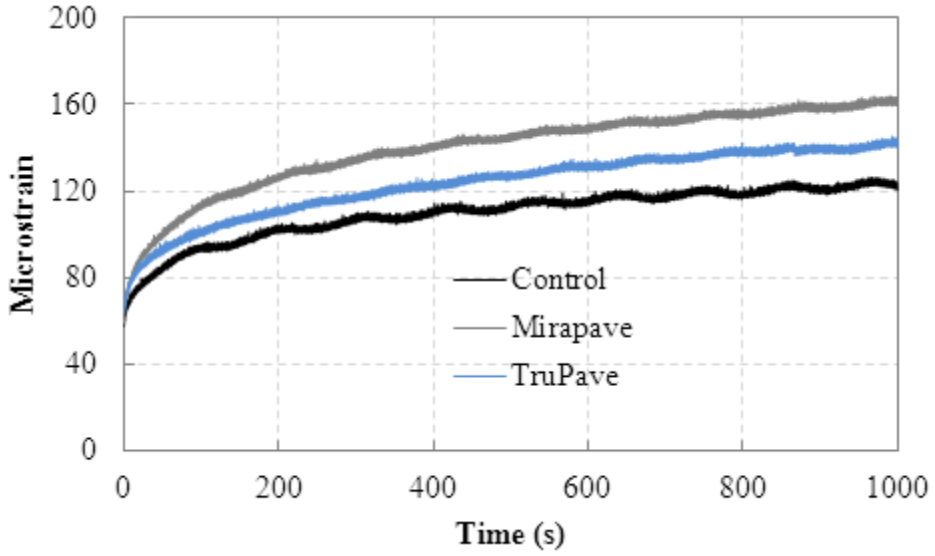


(d) -30°C, 12 kN vertical load

**Figure 2.23** Summary of horizontal creep strain

In the field, for an AC layer before cracking, decreasing temperature can increase the thermal stress in the AC layer. Under this situation, the paving interlayer may/may not contribute to carrying the tensile load, according to the results shown in Figure 2.23. However, when the AC layer cracks, the paving interlayer is expected to provide extra resistance to the widening of the crack due to the higher tensile strength it carries. This crack control capability cannot be revealed by the IDT creep test and will be explored in future research.

# CHAPTER 3 – FIELD MONITORING RESULTS AND ANALYSIS

In the previous project, *Performance of TenCate Mirafi PGM-G$^4$ Interlayer-Reinforced Asphalt Pavements in Alaska*, several types of paving interlayers provided by TenCate Geosynthetics were used to explore the performance of paving interlayer-reinforced asphalt concrete (AC) pavements in Alaska. Laboratory testing and finite element method (FEM) simulation identified a number of engineering benefits of using paving interlayers in AC pavements. To further validate the performance of paving interlayers in AC pavements in the field, the research team at the University of Alaska Fairbanks coordinated with ADOT&PF Northern Region personnel to select a pavement preservation/rehabilitation project (using a thin AC overlay), constructed during the summer season for establishment of test sections. This chapter presents field-related activities, including pre-construction field evaluation, establishment of test sections, and field evaluation after construction.

## Test Site Description

The test site starts at Milepost (MP) 148 on the Richardson Highway. The roadway consists of 2 inches of HMA (hot mix asphalt), 4 inches of ATB (asphalt-treated base), 4 inches of D-1 granular material, and about 3 feet of selected material. The selected material was crushed rock from the paving site. The first lift of 2 inches was paved in fall 2012.

## Pre-Construction Field Evaluation

A pre-construction field evaluation was conducted in May 2013. Cracks were observed on paved ATB after the snow melted from the roadway surface. The problematic areas were 1.4 mile to 6.7 mile from the beginning of the paving project. Most problematic areas had a weak foundation, and most cracks were longitudinal. Twelve cracking areas (Figures 3.1–3.13) were identified. Related detailed information is presented in Table 3.1. The pavement structure at the test section is shown in Appendix B.

**Table 3.1** Summary of pre-construction pavement survey

| ID | Mileage | Location | Length (ft) | Note | Suggestion |
|---|---|---|---|---|---|
| 1 | 1.4 | Longitudinal, Left lane, in the middle | 169 | | Can be used as a fabric test section. A 6 ft. wide fabric can cover the cracking area. |
| 2 | 1.6 | Longitudinal, mostly in the right lane, | 172 | Weak foundation | |
| 3 | 1.7 | Longitudinal, right lane, | 105 | Weak foundation, some on the shoulder | |
| 3a | 1.7 | Longitudinal, right lane, | 158 | Weak foundation, some on the shoulder | |
| 4 | 1.8 | Longitudinal, right lane | 283 | | Can be used as a control section |
| 5 | 1.9 | Longitudinal, right lane | 191 | On the shoulder | Not suggested as a test section, since it is on the shoulder. |
| 6 | 2.1 | Longitudinal, left lane | 142 | | Can be used as a fabric test section, which needs a 12 ft. wide fabric. |
| 7 | 3.5 | Longitudinal, left lane | 386 | most of the crack is on the longitudinal joint | |
| 8 | 3.6 | Longitudinal, left lane | 247 | including one transverse crack | Can be used as a fabric test section. It needs a 12 ft. wide fabric. |
| 9 | 3.8 | Longitudinal, left lane | 245 | | Can be used as a fabric test section. It needs a 6 ft. wide fabric. |
| 10 | 4.1 | Longitudinal, left lane | 478 | | Can be used as a control section and a fabric test section next to |

| ID | Mileage | Location | Length (ft) | Note | Suggestion |
|---|---|---|---|---|---|
| | | | | | each other for comparison. It needs a 12 ft. wide fabric. |
| 11 | 4.8 | Longitudinal, right lane | 293 | on the shoulder | Not suggested as a test section, since it is on the shoulder. |
| 12 | 6.7 | Longitudinal, left lane close to joint | 157 | | |

**Figure 3.1** Cracking area 1

**Figure 3.2** Cracking area 2

**Figure 3.3** Cracking area 3

**Figure 3.4** Cracking area 3a

**Figure 3.5** Cracking area 4

**Figure 3.6** Cracking area 5

**Figure 3.7** Cracking area 6

**Figure 3.8** Cracking area 7

**Figure 3.9** Cracking area 8

**Figure 3.10** Cracking area 9

**Figure 3.11** Cracking area 10

**Figure 3.12** Cracking area 11

**Figure 3.13** Cracking area 12

**Establishment of Test Sections**

Three test sections reinforced with paving interlayers were established in July 2013: one with $G^4$ in areas 2 and 3 (Figure 3.14), one with G50/50 in area 9 (Figure 3.15), and one with G100/100 in area 10 (Figure 3.16). A tack coat of neat oil was applied at the shooting rates of 0.19 gal/yd$^2$, 0.27 gal/yd$^2$, and 0.27 gal/yd$^2$ for sections with $G^4$, G50/50 and, G100/100, respectively. Area 4 was selected as the control section for further field survey. The pavement structures in four sections are presented in Figures 3.14 to 3.17.

(a) Construction of the test section

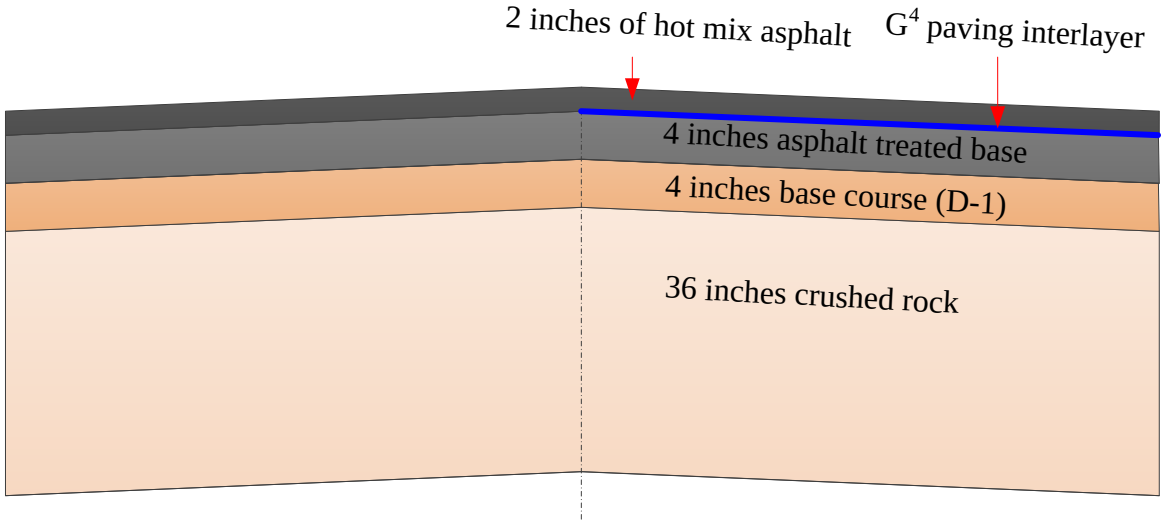


(b) Pavement structure

**Figure 3.14** $G^4$ test section

(a) Construction of the test section

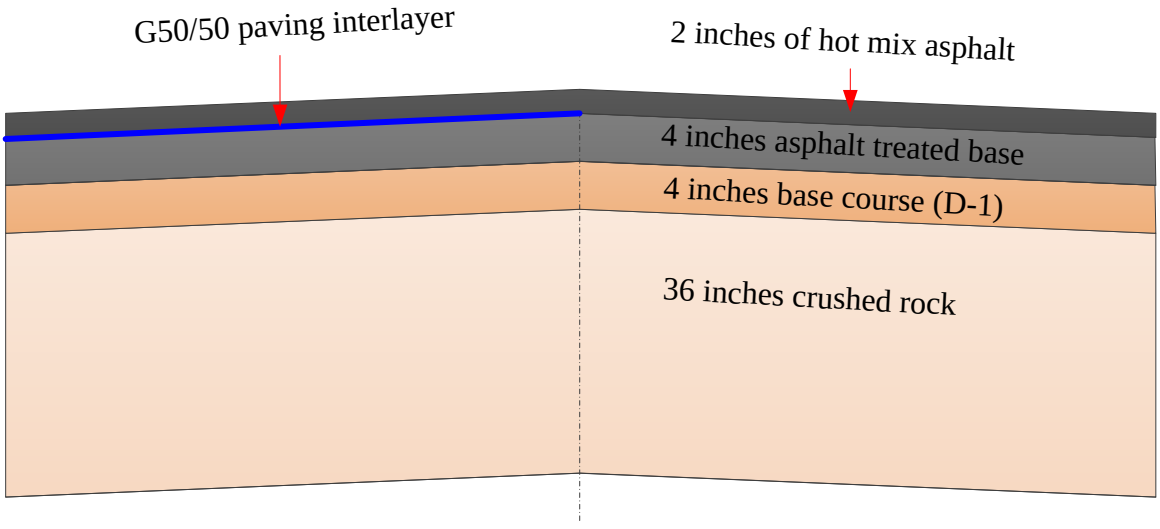


(b) Pavement structure

**Figure 3.15** G50/50 test section

(a) Construction of the test section

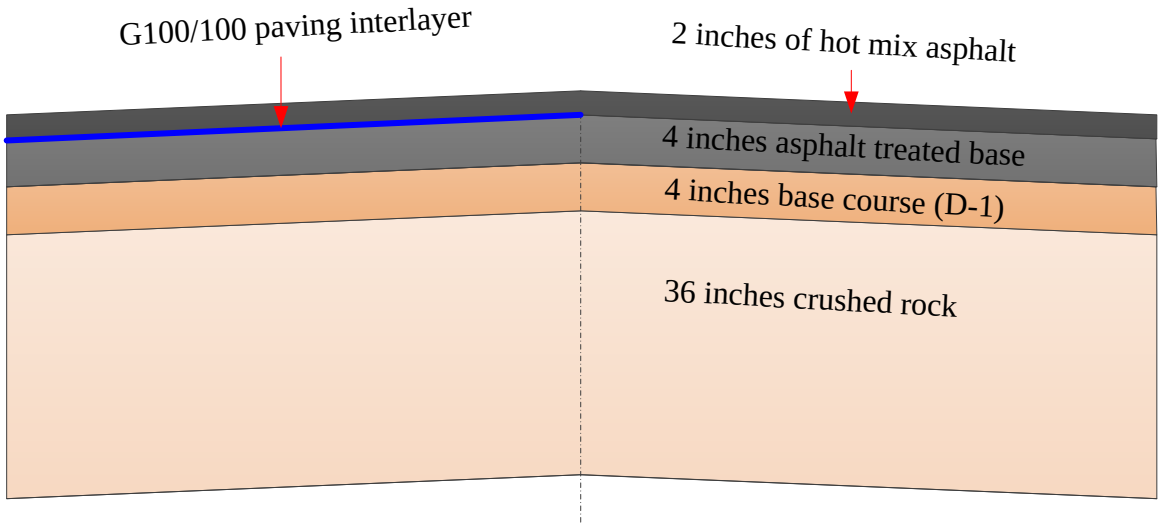


(b) Pavement structure

**Figure 3.16** G100/100 test section

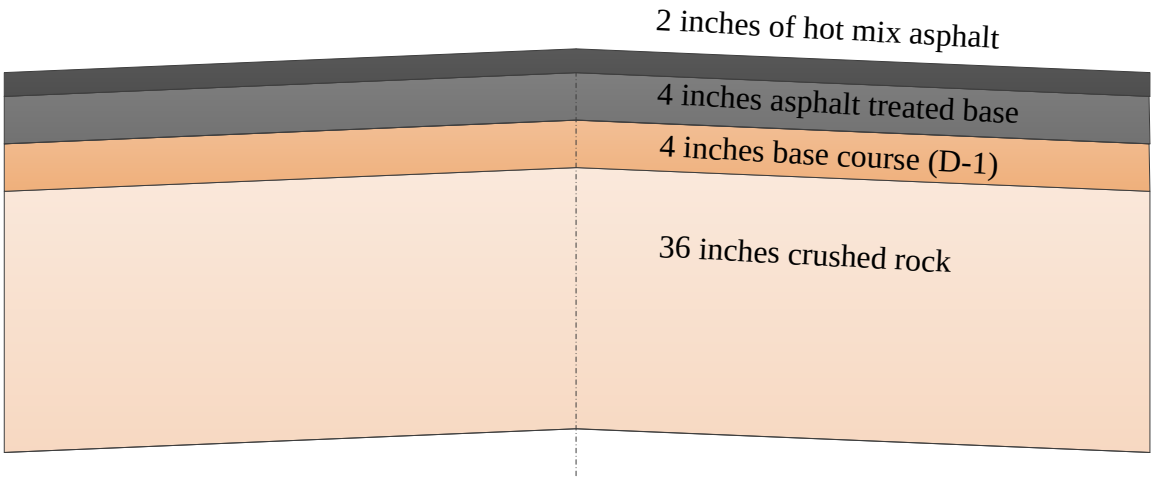


**Figure 3.17** Pavement structure of control section

## Field Climatic and Traffic Condition

The climatic data at the test section between the years 1981 and 2010 were collected from http://www.wrcc.dri.edu/. The average of all daily average temperatures recorded for the day of the year is presented in Figure 3.18a. According to the climatic data, the freezing and thawing indices were calculated to be -4779 freezing degree days (FDD) and 2226 thawing degree days (TDD) using Equations 3.1 and 3.2, respectively.

$$FDDs = \sum_{i=1}^{n} \left( T_{ave_i} - 32^{\circ}F \right), T_{ave_i} < 32^{\circ}F \tag{3.1}$$

$$TDDs = \sum_{i=1}^{n} \left( T_{ave_i} - 32^{\circ}F \right), T_{ave_i} > 32^{\circ}F \tag{3.2}$$

The traffic volume at the test section (from MP 148 to 156 of the Richardson Highway) is not available. However, the traffic volumes at Ernestine Maintenance Camp (MP 62 of the Richardson Highway) and Trims Maintenance Camp (MP 218 of the Richardson Highway) were collected from ADOT&PF. Since the test section is located at the middle of two stations, the

average of the data at two stations was used as the representative traffic volume at the test sections. The annual average daily traffic between the years 2010 and 2015 is presented in Figure 3.18b. The daily traffic did not vary much (from 361 per day to 382 per day) during this period. The annual traffic by month in 2015 is summarized in Figure 3.18c. The traffic volume in summer was approximately 4 times greater than in winter. The traffic by hour of day in 2015 is summarized in Figure 3.18d. The daily traffic peak was between 12:00 and 16:00 with average traffic volume of 30 per hour.

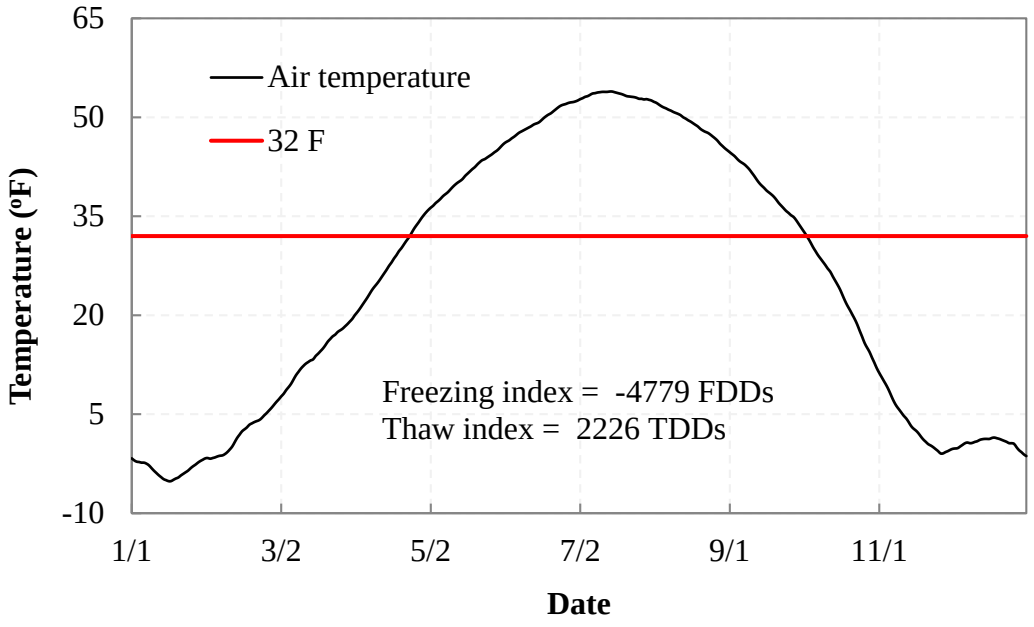


(a) Annual climatic condition

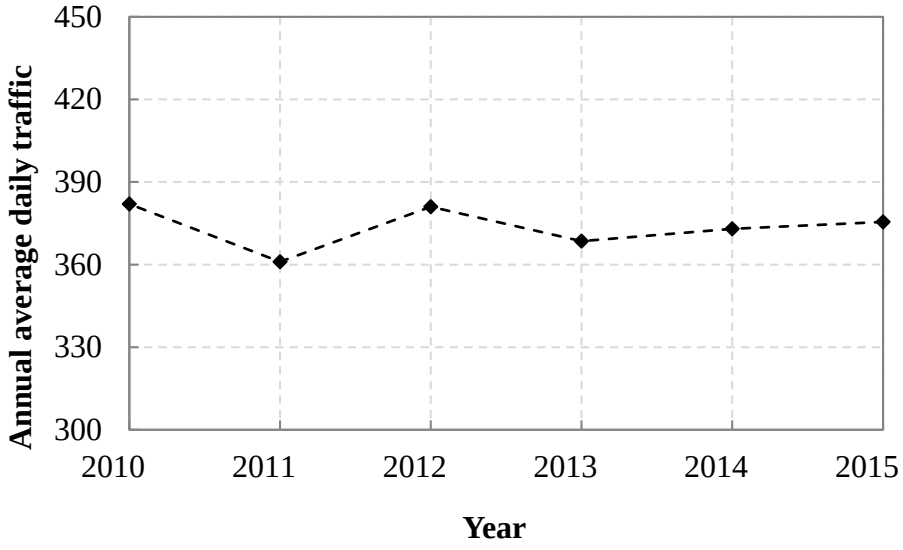


(b) Annual average daily traffic

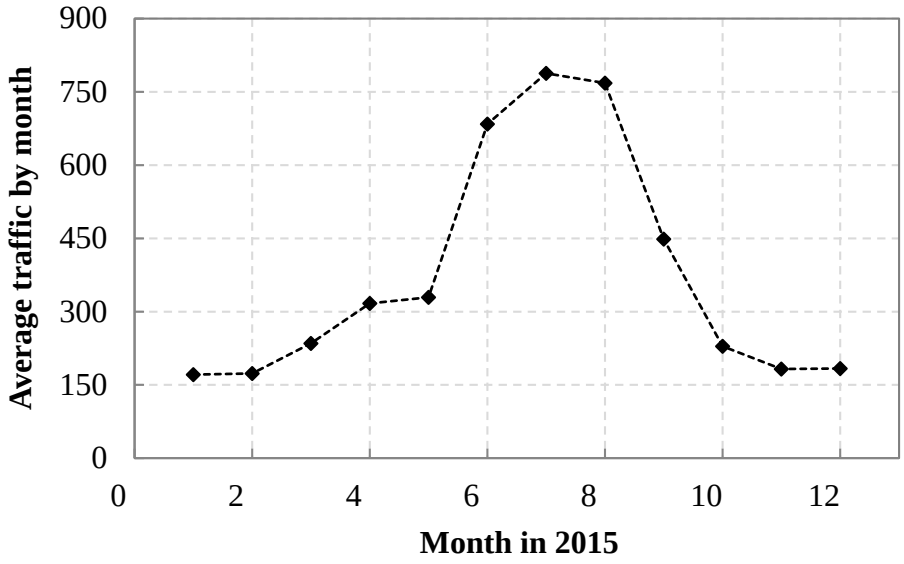


(c) Annual traffic by month

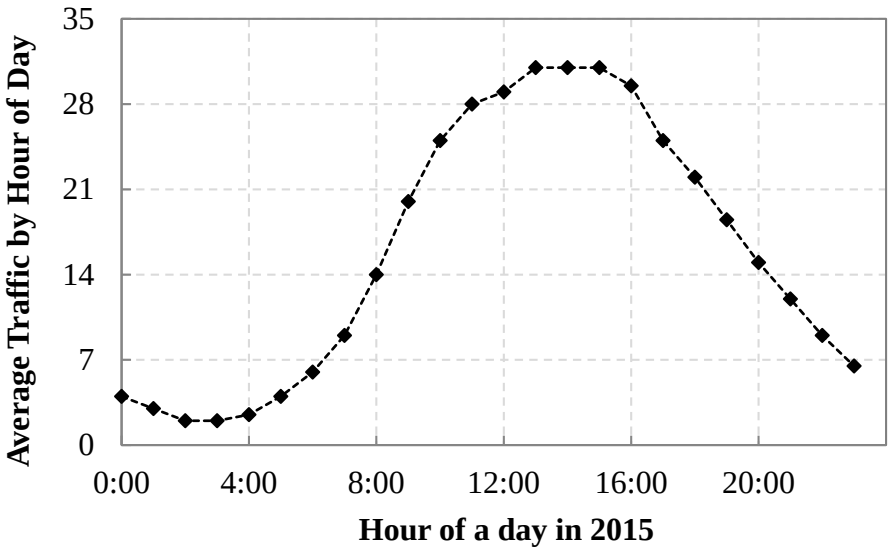


(d) Annual traffic by hour of day

**Figure 3.18** Climatic and traffic condition at the test section (1981–2010)

## Field Evaluation After Construction

### *Field Surveys in August and October 2013*

Two pavement condition surveys were conducted on August 19 and October 12, 2013. No cracks were found in any of the test sections during these two field trips (Figures 3.19–3.22).

**Figure 3.19** Control section (300 feet in area 4)

**Figure 3.20** $G^4$ test section (reinforced with 300 feet of $G^4$ paving interlayer in the right lane in area 2, no visible cracks)

**Figure 3.21** G50/50 test section (reinforced with 300 feet of G50/50 in the left lane in area 9, no visible cracks)

**Figure 3.22** G100/100 test section (reinforced with 300 feet G100/100 in the left lane in area 10, no visible cracks present)

***Field Survey in May and September 2014***

Field evaluations were performed on May 15 and in September 2014 to see how the paving interlayers had functioned over the course of the winter. Cracks were observed in every test section (Figures 3.23–3.26). Table 3.2 summarizes the crack data collected.

(a)

(b)

**Figure 3.23** Control section: (a) no visible cracks (October 12, 2013); (b) 266 feet of longitudinal crack (May 15, 2014)

(a)

(b)

**Figure 3.24** $G^4$ test section: (a) no visible cracks (October 12, 2013); (b) both longitudinal and transverse cracks present (May 15, 2014)

(a)

(b)

**Figure 3.25** G50/50 test section: (a) no visible cracks (October 12, 2013); (b) both transverse and longitudinal cracks present (May 15, 2014)

(a)

(b)

**Figure 3.26** G100/100 test section: (a) no visible cracks (October 12, 2013); (b) transverse crack present (May 15, 2014)

**Table 3.2** Summary of crack data in September 2014

| Section | Transverse crack (#) | Longitudinal crack, Right lane (ft) | Longitudinal crack, Left lane (ft) |
|---|---|---|---|
| Area 4 (control) | 0 | 266 medium-major | 0 |
| Areas 2 & 3 | 3 minor | 17 minor ($G^4$) | 0 |
| Area 9 | 1 | 28 minor | 36 minor (G50/50) |
| Area 10 | 1 | 0 | 0 (G100/100) |

The control section (area 4) was by far the worst with 89% of the northbound lane carrying a 266-foot medium-severity longitudinal crack. The northbound lane of area 2, which had been reinforced with $G^4$ paving interlayer, had one full-length transverse crack and two other cracks that started from the shoulder and crossed the northbound lane, ending at the centerline. Small transverse cracks between 274 and 294 feet were observed from the start of the $G^4$ section in the center of the northbound lane. The southbound lane of area 9 is the section that was reinforced with G50/50. A transverse crack was observed 160 feet from the start of the G50/50 section. The first part of the southbound lane of area 10 is the 300 foot G100/100 reinforced section. Only one full-length transverse crack, located about 117 feet from the start of the reinforcement, was observed.

According to the summary in Table 3.2, all sections reinforced with paving interlayers performed better (reduced number and severity of cracks) than the control section. In terms of number and severity level of cracks, the section reinforced with G100/100 performed the best, followed by the $G^4$ section and the G50/50 section. That the $G^4$ section showed more cracks than the G100/100 section may be due to the weak foundation in areas 2 and 3 (see Table 3.2), where the $G^4$ section was located. Another observation from the pavement survey was that many of the transverse cracks were located at the possible interlayer joints. During construction of the test sections, all paving interlayers were cut to lengths of about 300 feet for easy installation, which may have caused weak spots for stress concentration and crack occurrence in the interlayer sections.

This possibility can be avoided in real-life construction where paving interlayers are laid out continuously as an entire layer.

In September 2014, the $G^4$ reinforced section (area 2) had the only new crack found in all of the test sections, and it was minor (Figure 3.27–3.29). Many very small fissures were observed where likely, after the next winter, more cracks would become pronounced. Overall, the test sections including the control sections were in the same condition as the evaluation performed in May 2014.

**Figure 3.27** Control section (area 4) no new crack

**Figure 3.28** $G^4$ section (area 2) new minor crack

**Figure 3.29** G50/50 and G100/100 (sections 9 and 10) no new crack

***Field Survey in June 2015***

A field evaluation was performed and crack data were collected on June 2, 2015. Crack data collected from the survey conducted in May 2014 and this survey are summarized and presented in Table 3.3. Figures 3.30–3.33 show the typical new cracks in every test section.

**Table 3.3** Summary of crack data in June 2015

| Section | | Transverse crack (#) | Longitudinal crack, Right lane (ft) | Longitudinal crack, Left lane (ft) |
|---|---|---|---|---|
| Area 4 (control) | Previous | 0 | 266 medium-major | 0 |
| | New | 7 minor | 34 medium-major<br>13 minor | 0 |
| | Total | 7 minor | 300 medium-major<br>13 minor | 0 |
| Areas 2 & 3 | Previous[1] | 3 minor | 17 minor ($G^4$) | 0 |
| | New[2] | 5 minor | 46 minor ($G^4$) | 14 minor |
| | Total | 8 minor | 63 minor ($G^4$) | 14 minor |
| Area 9 | Previous | 1 major | 28 minor | 36 minor (G50/50) |
| | New | 0 | 50 minor | 24 minor (G50/50) |
| | Total | 1 major | 78 minor | 60 minor (G50/50) |
| Area 10 | Previous | 1 major | 0 | 0 (G100/100) |
| | New | 0 | 0 | 0 (G100/100) |
| | Total | 1 major | 0 | 0 (G100/100) |

[1] *Previous − Data collected as of May 2014.*

[2] *New − Data collected in June 2015.*


(a)

(b)

**Figure 3.30** Control section: (a) new minor transverse crack; (b) new moderate-major longitudinal crack

(a)

(b)

**Figure 3.31** $G^4$ test section: (a) new minor transverse crack; (b) new minor longitudinal crack


(a)

(b)

**Figure 3.32** G50/50 test section: (a) no new transverse crack; (b) new minor longitudinal crack

(a)

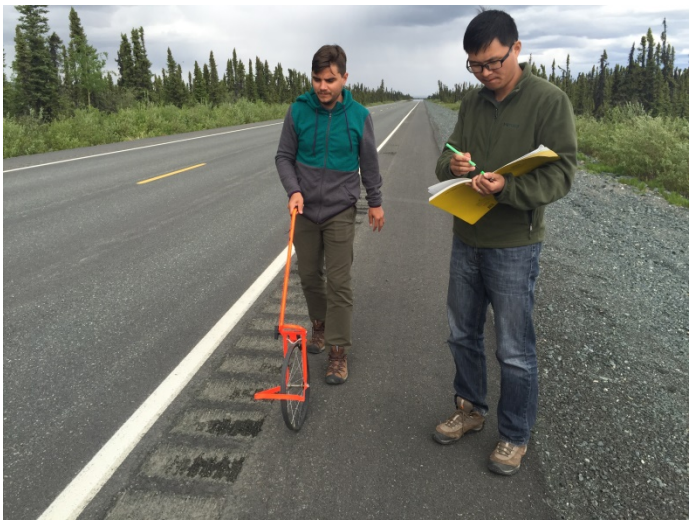

(b)

**Figure 3.33** G100/100 test section: (a) no new transverse crack; (b) no new longitudinal crack

In Table 3.3, it can be seen that the control section showed the worst longitudinal crack performance in terms of number of new cracks and severity after 1 year of service. Most new transverse cracks were found on the control section rather than on sections reinforced by paving interlayers. The $G^4$ reinforced section showed several newly formed minor transverse and longitudinal cracks, while new minor longitudinal cracks were observed on the G50/50 section only. The G100/100 section performed the best without any new cracks observed.

As discussed previously, the additional cracks observed on the $G^4$ section rather than the G100/100 section may be due to the weak foundation in areas 2 and 3 where the $G^4$ section was located. Note that plenty of transverse cracks were found at the possible joints of each 300-foot paving interlayer during construction. The stress concentration at the joints may have caused the cracks, other than the effects of the paving interlayers. These factors may have affected the surveys conducted in this study, but could be avoided in real-life construction.

***Field Survey in June 2016***

A field evaluation was performed on June 24, 2016. Table 3.4 presents new data collected from this survey and previous data as of the last field survey 1 year ago. In Table 3.4, it can be seen that after 1 year's service, four more minor transverse cracks were observed on the control section, while two new minor cracks were observed on the $G^4$ section. No transverse crack has been observed on the G50/50 and G100/100 sections since the 2014 survey. A few longitudinal cracks were found on all sections.

**Table 3.4** Summary of crack data in June 2016

| Section | | Transverse crack (#) | Longitudinal crack, Right lane (ft) | Longitudinal crack, Left lane (ft) |
|---|---|---|---|---|
| Area 4 (control) | Previous[1] | 7 minor | 300 medium-major<br>13 minor | 0 |
| | New[2] | 4 minor | 4 medium-major | 0 |
| | Total | 11 minor | 304 medium-major<br>13 minor | 0 |
| Areas 2 & 3 | Previous | 8 minor | 63 minor ($G^4$) | 14 minor |
| | New | 2 minor | 14 minor ($G^4$) | 0 |
| | Total | 10 minor | 77 minor ($G^4$) | 14 minor |
| Area 9 | Previous | 1 major | 78 minor | 60 minor (G50/50) |
| | New | 0 | 0 | 20 minor (G50/50) |
| | Total | 1 major | 78 minor | 80 minor (G50/50) |
| Area 10 | Previous | 1 major | 0 | 0 (G100/100) |
| | New | 0 | 20 minor | 0 (G100/100) |
| | Total | 1 major | 20 minor | 0 (G100/100) |

[1] *Previous − Data collected before June 2015.*

[2] *New − Data collected in June 2016.*

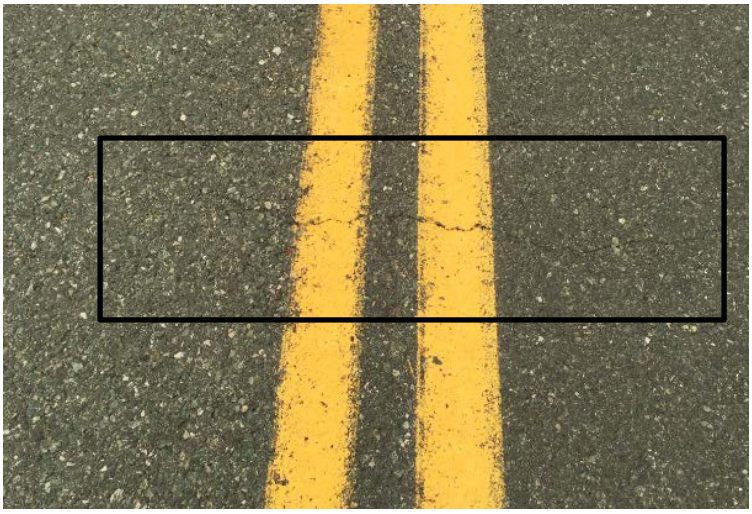

(a)

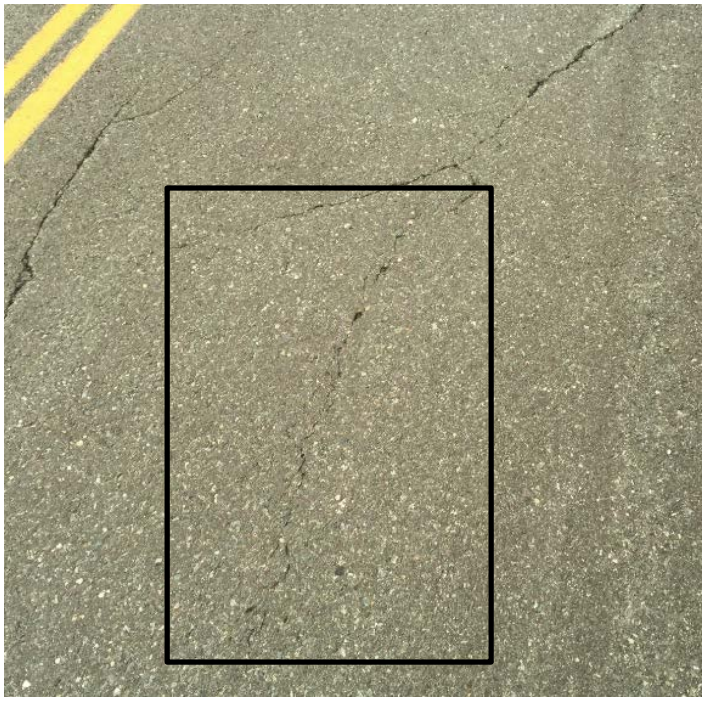

(b)

**Figure 3.34** Control section: (a) new minor transverse crack; (b) new moderate-major longitudinal crack

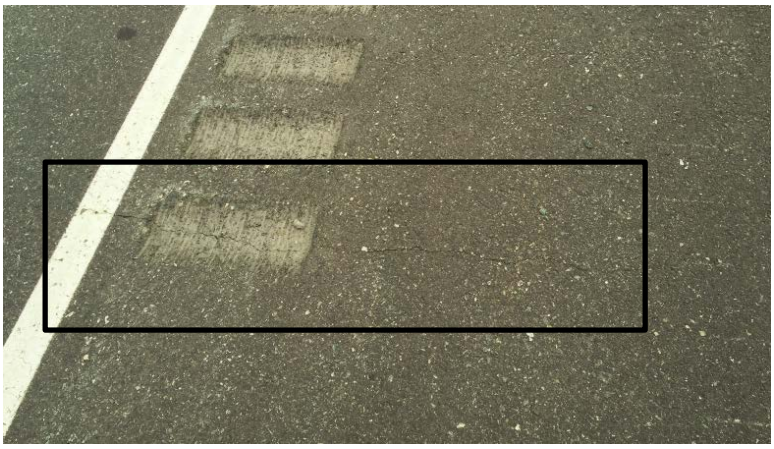

(a)

(b)

**Figure 3.35** $G^4$ test section: (a) new minor transverse crack; (b) new minor longitudinal crack

(a)

(b)

**Figure 3.36** G50/50 test section: (a) no new transverse crack (but polishing is very obvious); (b) new minor longitudinal crack on the shoulder

(a)

(b)

**Figure 3.37** G100/100 test section: (a) no new transverse or longitudinal crack (but polishing is very obvious); (b) the major crack observed from May 2014, 1/8 to 1 in width

***Field Survey in May 2017***

On May 9, 2017, a field evaluation was performed. Table 3.5 presents new data collected from this survey and previous data as of the last field survey a year ago. After 1 year, no new transverse crack was observed on all sections. The new medium-major transverse crack in areas 2 and 3 evolved from a minor transverse crack, as shown in Figure 3.38. The width of the transverse crack in the G50 sections did not increase according to Figure 3.39. However, note that the length of some transverse cracks did increase (see Figure 3.40). Also, a few longitudinal cracks were found on the control, $G^4$, G50/50, and G100/100 sections. The distributions of previous and new cracks in all sections are presented in Appendix C.

**Table 3.5** Summary of crack data in May 2017

| Section | | Transverse crack (#) | Longitudinal crack, Right lane (ft) | Longitudinal crack, Left lane (ft) |
|---|---|---|---|---|
| Area 4 (control) | Previous[1] | 11 minor | 304 medium-major<br>13 minor | 0 |
| | New[2] | 0 | 5 medium-major | 0 |
| | Total | 11 minor | 309 medium-major<br>13 minor | 0 |
| Areas 2 & 3 | Previous | 10 minor | 77 minor ($G^4$) | 14 minor |
| | New | 1 medium-major | 20 minor ($G^4$) | 0 |
| | Total | 9 minor<br>1 medium-major | 97 minor ($G^4$) | 14 minor |
| Area 9 | Previous | 1 major | 78 minor | 80 minor (G50/50) |
| | New | 0 | 36 minor | 20 minor (G50/50) |
| | Total | 1 major | 114 minor | 100 minor (G50/50) |
| Area 10 | Previous | 1 major | 20 minor | 0 (G100/100) |
| | New | 0 | 42 minor | 0 (G100/100) |
| | Total | 1 major | 62 minor | 0 (G100/100) |

*[1] Previous − Data collected before June 2016; [2] New − Data collected in May 2017.*

**Figure 3.38** Evolution of a transverse crack from minor to major in $G^4$ test section


**Figure 3.39** A transverse crack in G50/50 section

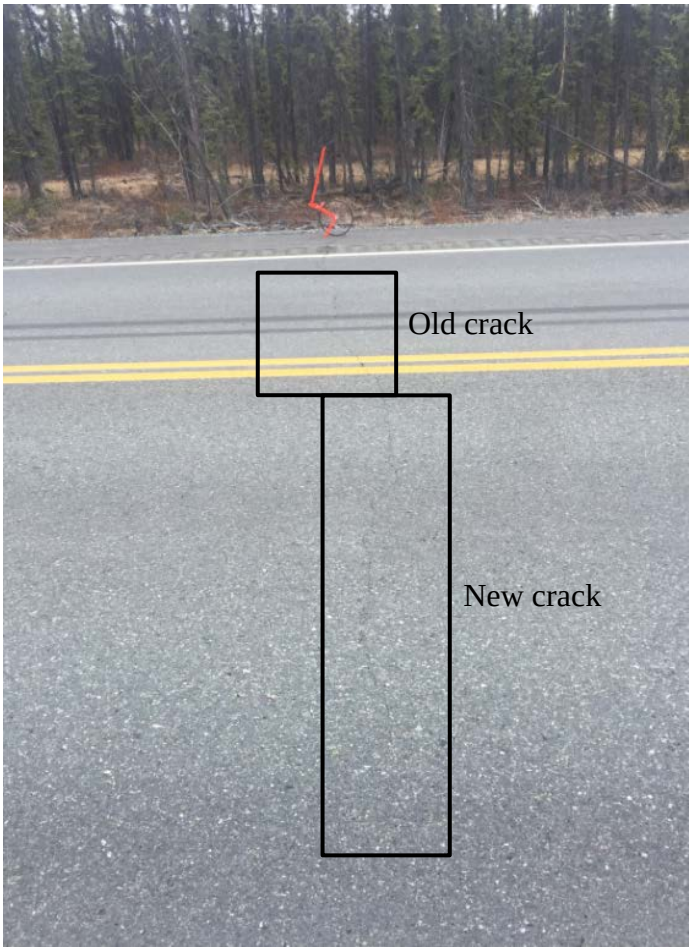


**Figure 3.40** Evolution of a transverse crack in $G^4$ test section

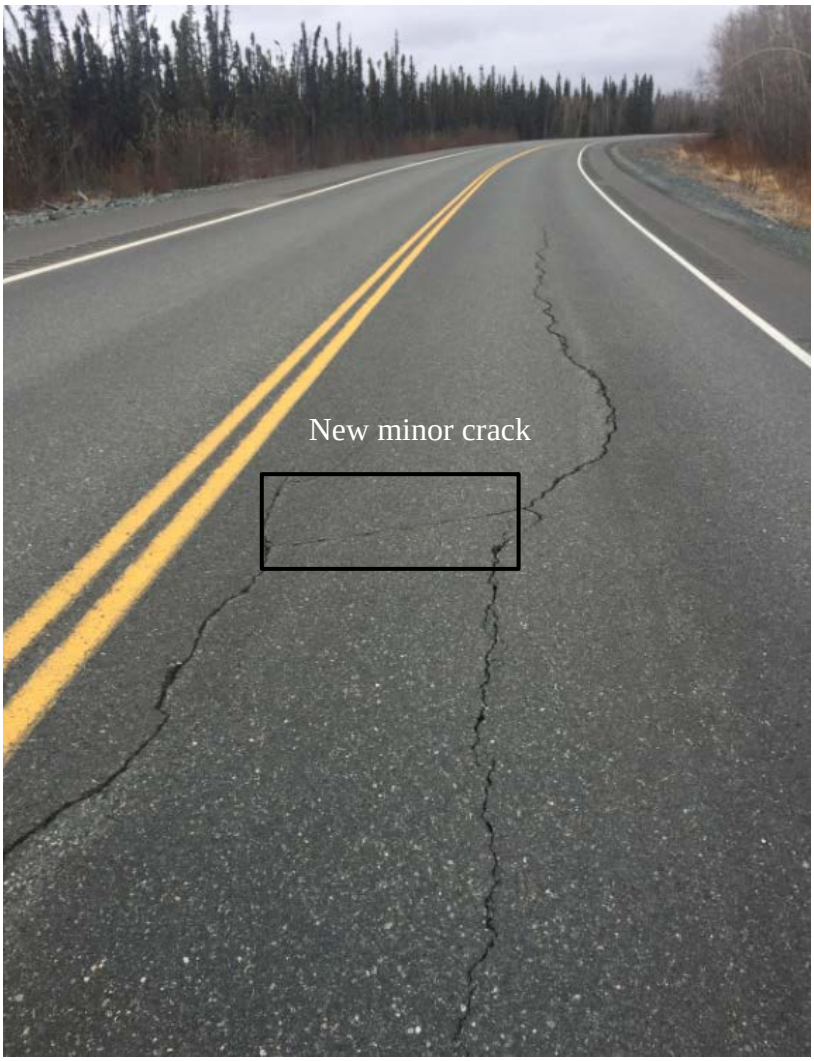


**Figure 3.41** New minor crack in the control section

**Pavement Data from ADOT&PF**

Pavement data were collected according to the Highway Performance Monitoring System (HPMS), a national highway information system that includes data on the extent, condition, performance, use, and operating characteristics of the nation's highways. The collected data only cover the right lane of the pavement. In three sections paved with fabric, only the $G^4$ section was located at the right lane; hence, the results presented in Figure 3.42 only cover the control and $G^4$

sections. The international roughness index (IRI) and rutting depth in the control section were slightly lower than those in the $G^4$ section.

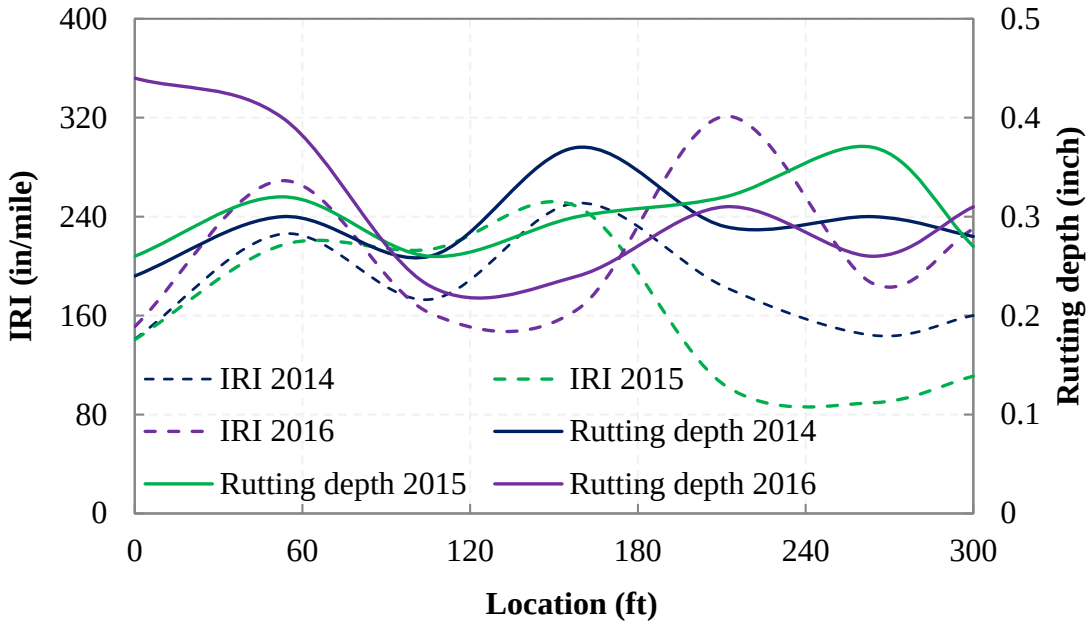


(a) $G^4$ section

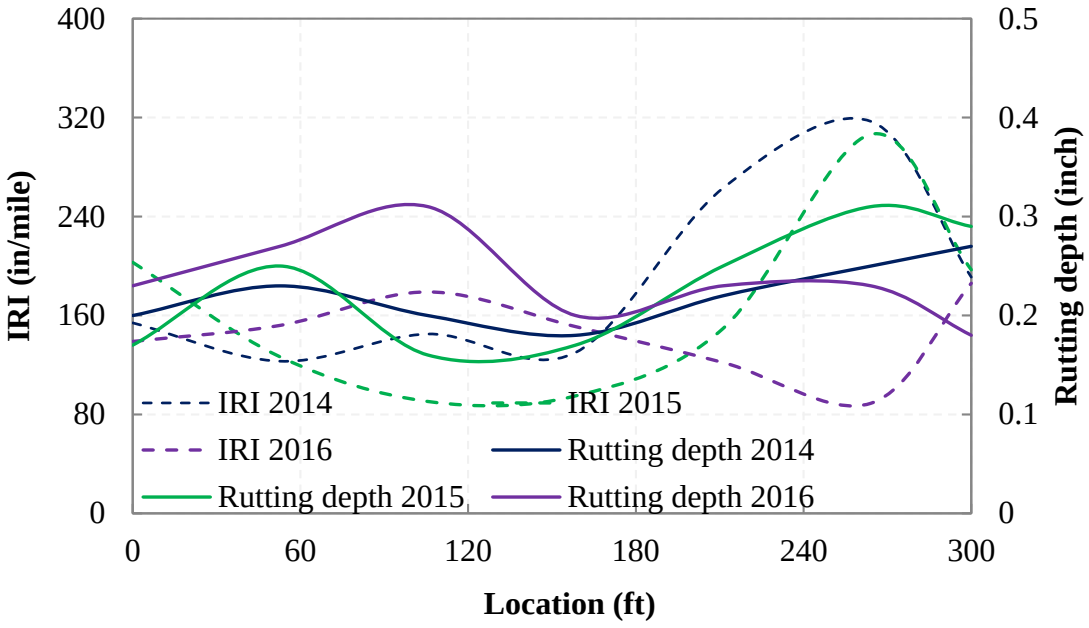


(b) Control section

**Figure 3.42** Pavement IRI and rutting depth between 2014 and 2016

In addition to IRI and rutting depth, cracking length and percentage were collected. Cracking length is the total length of transverse cracks within the sample area, and cracking percentage is defined as the percentage of the total area exhibiting visible fatigue-type cracking for all severity levels in the wheel path in each section. The cracking length and percentage for the $G^4$ and control sections are presented in Figures 3.43a and 3.43b. Both cracking length and percentage in the $G^4$ section were less than those in the control section, indicating that the use of $G^4$ increased pavement crack resistance, which is consistent with the survey result.

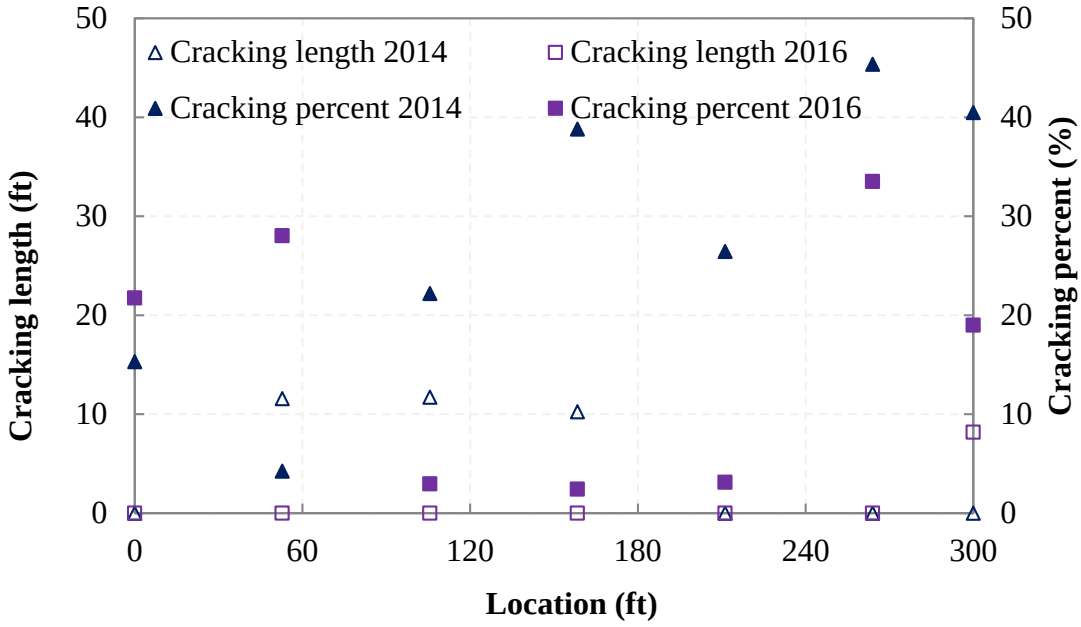


(a) $G^4$ section

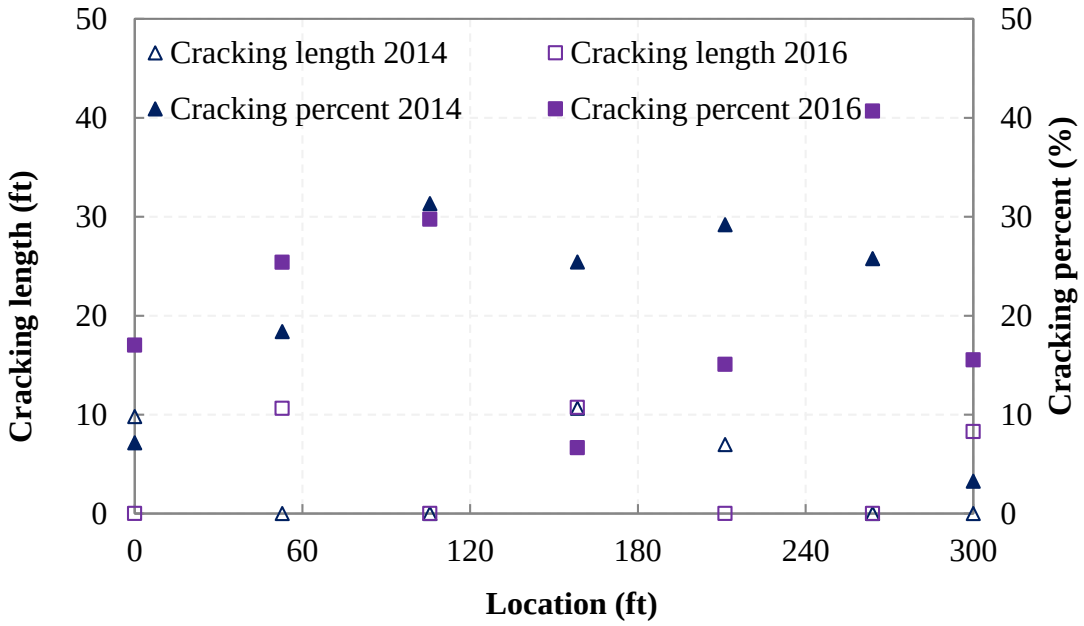


(b) Control section

**Figure 3.43** Pavement cracking length and percent in 2014 and 2016

# CHAPTER 4 – CONCLUSIONS

The performance of two paving interlayers—Mirapave and TruPave—was evaluated through a series of laboratory tests: an overlay test, dynamic modulus test using AMPT, dynamic modulus test in IDT mode, and IDT creep test. A field survey of the field test sections on the Richardson Highway was performed to evaluate the performance of three sections of AC pavement that had been reinforced with paving interlayers ($G^4$, G50/50, and G100/100). Several conclusions were drawn:

1. The overlay test results on the AC reinforced with two paving interlayers (Mirapave and TruPave) indicated that samples with an entire layer of TruPave material show the highest peak load reduction percentage at the same loading cycles, followed by the control samples, then the other three groups (AC with TruPave interlayer strip, Mirapave interlayer strip, and entire Mirapave interlayer). The mixtures with paving interlayers (Mirapave and TruPave) generally showed better performance in crack resistance. Note that TruPave was adhesive on one-side only. The overlay test setup could have largely amplified the bonding weakness between the TruPave entire layer and the AC during the test, causing the early failure. More should be done to verify this finding.
2. The dynamic modulus test using an AMPT produced very low |E*| for specimens with paving interlayers due to the inclusion of the paving interlayer and its low stiffness. The AMPT was considered inappropriate, since the paving interlayer in this test was under compression rather

than tension, which is different from the stress state that the interlayer would experience in the field when used for cracking mitigation purposes.

3. The |E*| was also measured in IDT mode. The obtained |E*| master curves of the control mixture tested using two methods (AMPT and IDT mode) were very close, which verified the rationality of the dynamic modulus measurement in IDT mode. The master curves of the TruPave and Mirapave mixtures were close to that of the control mixture, which was different from the |E*| results from the AMPT. According to the results presented in this study, in terms of dynamic modulus measurement, the IDT mode is preferable to the AMPT method due to the similar stress state that the fabric would experience in the field.
4. The IDT creep test results revealed that the creep compliances were significantly influenced by testing temperature. When the temperature decreased from 20°C to -10°C, the creep compliance of AC with/without paving interlayers dramatically decreased. At low temperature (i.e., -30°C), the creep compliances of mixtures with paving interlayers were comparable to the control mixtures. As a result, the inclusion of paving interlayers in the pavement structure did not compromise pavement performance in low-temperature cracking resistance. Note that the variation in creep compliance of the control group was more dramatic than that of the mixtures with paving interlayers. Adding paving interlayer to the AC could reduce the temperature sensitivity of the material. Besides these, the IDT creep test results show that the creep strain of the AC with paving interlayers could be higher or lower than that of the control groups at different temperatures. That is, the paving interlayer may/may not contribute to carrying the

tensile load before the cracking of AC. However, when an AC layer cracks, the paving interlayer is expected to provide extra resistance to the widening of the crack due to the higher tensile strength it can carry. This crack control capability cannot be revealed by the IDT creep test and will be explored in future research.

5. In addition to the laboratory test, a yearly survey was performed on the field sections after the construction in 2013. After 4 years of surveying and monitoring, it can be observed that all test sections reinforced with paving interlayers (G50/50, G100/100, and $G^4$) showed better pavement performance than the control section, which indicates that the placement of paving interlayers selected in this study would benefit pavement performance. Among the sections with paving interlayers built in, the G100/100-reinforced pavement showed the best performance, followed by the G50/50-reinforced section, then the $G^4$ section.
6. As for the field survey results, it is still early to draw any conclusion about the paving interlayer effects, as 4 years is typically considered a short period in the entire life cycle of pavement. In addition, a few construction issues were noticed that may have affected the survey results. Therefore, it is our recommendation that field cores be collected from the sites at which the cracking occurred, in order to reveal more information underground. We also recommend continued monitoring of the test sections, with more detailed description of pavement distress, to see how the pavement progresses with time. Having a few more years' data would provide a much clearer projection of the utility of paving interlayers in cold regions.

## REFERENCES

AASHTO T-322 (2008). "Standard Method of Test for Determining the Creep Compliance and Strength of Hot-Mix Asphalt (HMA) Using the Indirect Tensile Test Device." American Association of State and Highway Transportation Officials.

AASHTO TP-62 (2008). "Standard Method of Test for Determining Dynamic Modulus of Hot Mix Asphalt." American Association of State and Highway Transportation Officials.

AASHTO TP-79 (2008). "Standard Method of Test for Determining the Dynamic Modulus and Flow Number for AC Using the Asphalt Mixture Performance Tester (AMPT)." American Association of State and Highway Transportation Officials.

AKFPD (2004). Alaska Flexible Pavement Design Manual. Alaska Department of Transportation and Public Facilities.

ARA, Inc. (2000). "Guide for Mechanistic-Empirical Design of New and Rehabilitated Pavement Structures, Appendix DD-1: Resilient modulus as function of soil moisture – Summary of predictive models." NCHRP Rep. No. A-37A, Transportation Research Board, Washington, DC.

ASTM D7329 (2004) "Standard Specification for Hybrid Geosynthetic Paving Mat for Highway Applications." ASTM International, West Conshohocken, PA.

Germann, F.P., and Lytton, R.L. (1979). "Methodology for Predicting the Reflection Cracking Life of Asphalt Concrete Overlays. Research Report FHWA/TX-79/09+207-5, Texas Transportation Institute, Texas A&M University, College Station, TX.

Kim, Y., Seo, Y., King, M., and Momen, M. (2004). “Dynamic modulus testing of asphalt concrete in indirect tension mode.” Transportation Research Record: *Journal of the Transportation Research Board* (1891), 163–173.

Li., P., Liu, J., and Eckman., P. (2014). “Performance of TenCate Mirafi PGM-G4 Interlayer-Reinforced Asphalt Pavements in Alaska.” Alaska University Transportation Center, Project Number 12069.

Zhou, F., and Scullion, T. (2005). “User Manual for TxDOT’s New Overlay Tester.” Texas Transportation Institute, Texas A & M University System.

## APPENDIX A: JMF of Rich Hwy North Pole Interchange Paving Project

STATE OF ALASKA - NORTHERN REGION
DEPARTMENT OF TRANSPORTATION AND PUBLIC FACILITIES
BITUMINOUS MIX DESIGN MARSHALL METHOD
2301 PEGER ROAD
FAIRBANKS, AK 99709

RECEIVED: 6/18/2008
COMPLETE: 5/25/2008

| | | | |
|---|---|---|---|
| PROJECT NAME: | Rich Hwy North Pole Interchange | REGIONAL LAB # : | 08-246 |
| PROJECT NUMBER: | ACIM-0A2-4(26) | FIELD # : | NPI-HMA-MD-1 |
| LEDGER CODE: | 30388942 / 62184 | TYPE/CLASS: | II B |

| | |
|---|---|
| AGGREGATE SOURCE: | 900 Old Rich |
| AGGREGATE QUALITY#: | 06-067 |
| BLEND RATIO: | 23:23.5:42:11.5 CA:INT:FA:SA |
| BLENDED BULK SPG: | 2.677 |
| EFFECTIVE SPG: | 2.706 |

| | |
|---|---|
| BINDER SOURCE: | EPA |
| BINDER GRADE: | PG 64-34 |
| BINDER SPG: | 1.0016 |
| ANTISTRIP: | .25% |

| MIX DESIGN PARAMETERS | |
|---|---|
| STABILITY | 1200 |
| FLOW | 8-16 |
| VOIDS TOTAL MIX | 3-5 |
| COMPACTION, BLOWS | 50 |
| VOIDS FILLED | 65-78 |
| VMA | 12 |
| DUST RATIO | .6-1.4 |

| | |
|---|---|
| MIXING TEMP (DEG F) | 302 |
| COMPACTING TEMP (DEG F) | 295 |

| MARSHALL RESULTS | |
|---|---|
| % ASPHALT @ MAX UNIT WT | 6.5 |
| % ASPHALT @ MAX STABILITY | 6 |
| % ASPHALT @ 4% VOIDS | 5.4 |
| **OPTIMUM OIL CONTENT = 5.4 %** | |
| STABILITY | 2375 |
| FLOW | 9.7 |
| VOIDS TOTAL MIX | 4 |
| VOIDS FILLED | 74 |
| VMA | 16 |
| MTD/RICE | 2.483 |
| DUST ASPHALT RATIO | 0.7 |

APPROVED:

| AGGREGATE DESIGN PARAMETERS | | |
|---|---|---|
| | | Spec |
| F&E | 0% | 8%max |
| LL | NV | |
| PI | NP | |
| T304 | | |
| FRACTURE | 98% | 90%df |

| SIEVE SIZE | PROPOSED GRADATION | MIX DESIGN SPEC BAND | |
|---|---|---|---|
| | | LSL | HSL |
| 1" | | ----- | ----- |
| 3/4" | | ----- | ----- |
| 1/2" | 87 | 81 | 93 |
| 3/8" | 74 | 68 | 80 |
| #4 | 52 | 46 | 58 |
| #8 | 39 | 33 | 45 |
| #10 | | ----- | ----- |
| #16 | 30 | 25 | 35 |
| #20 | | ----- | ----- |
| #30 | 25 | 21 | 29 |
| #40 | | ----- | ----- |
| #50 | 19 | 15 | 23 |
| #60 | | ----- | ----- |
| #80 | | ----- | ----- |
| #100 | 8 | 5 | 11 |
| #200 | 3.5 | 1.5 | 5.5 |

REMARKS:

# APPENDIX B: Site Section Pavement Structure

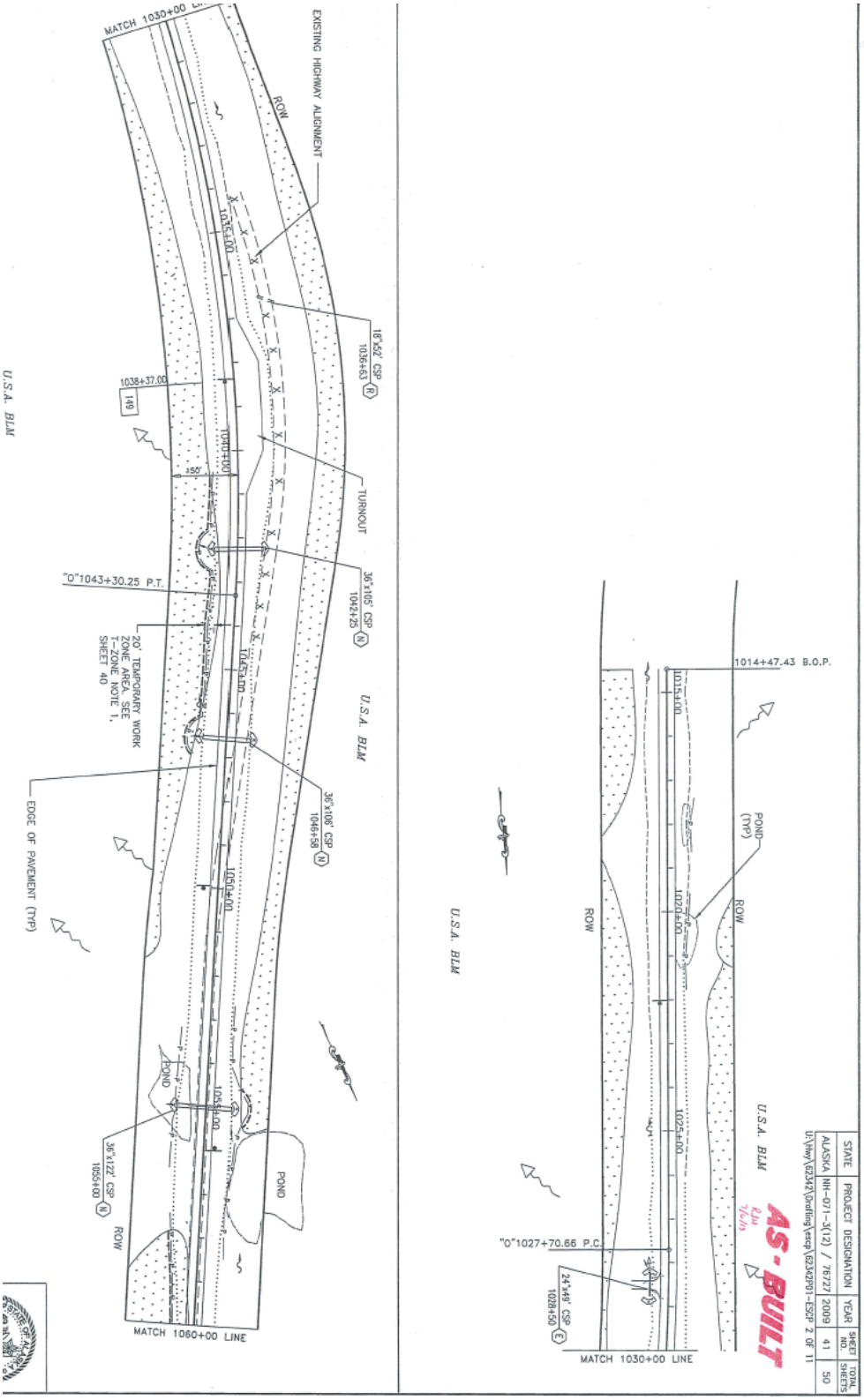

MATCH 1090+00 LINE
MATCH 1120+00 LINE
MATCH 1060+00 LINE
MATCH 1090+00 LINE
ROW
POND
CABIN
CABINS
LAKE
EXISTING HIGHWAY ALIGNMENT
U.S.A. BLM
SECTION 13
SECTION 24
SECTION 18
"0"1070+67.70 P.C.
"0"1073+23.21 P.T.
"0"1088+47.00 P.C.
AS - BUILT
ESCP 3 OF 11
STATE
ALASKA
PROJECT DESIGNATION
NH-071-3(12) / 76727
YEAR
2009
SHEET NO.
42
TOTAL SHEETS
50

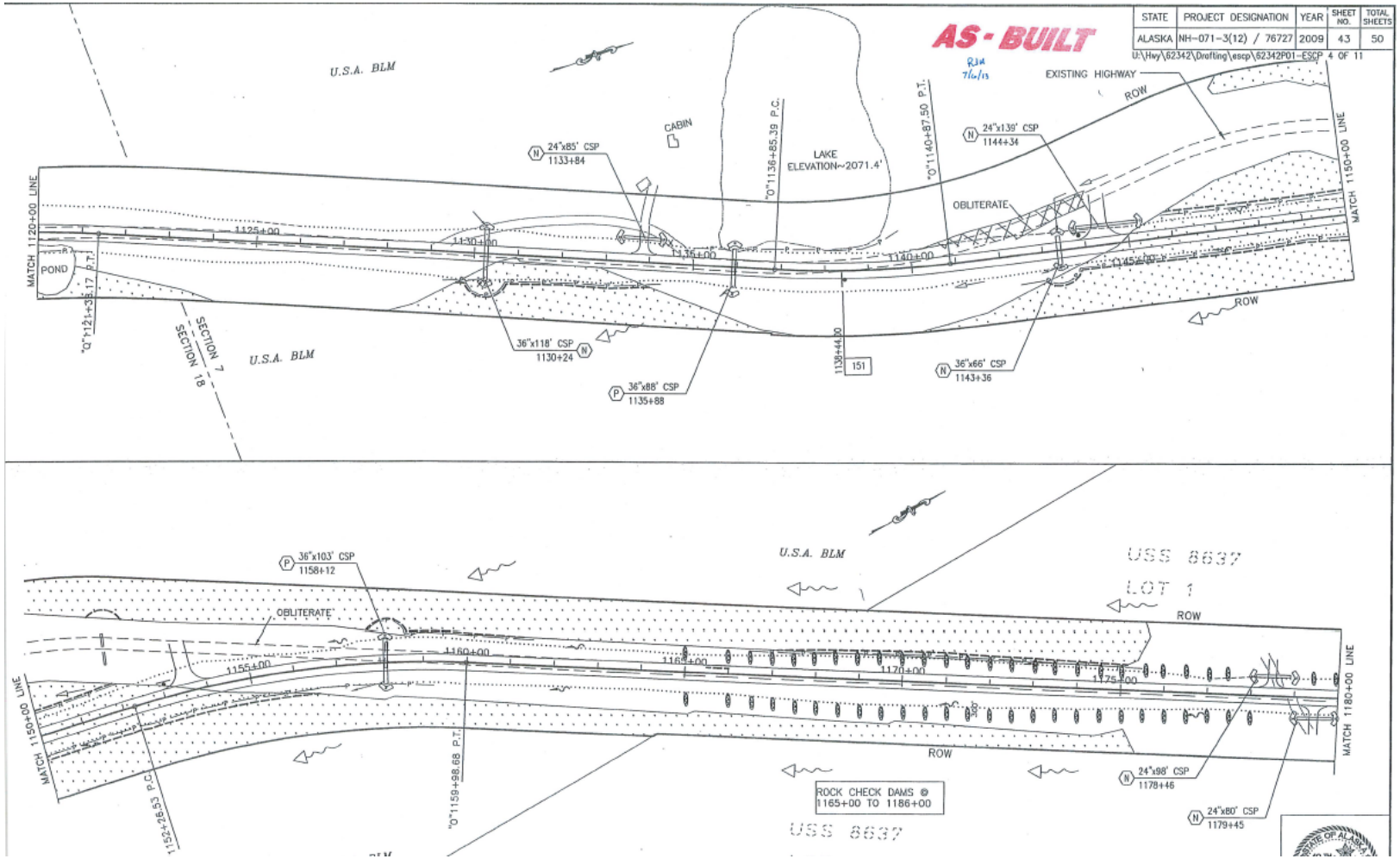
AS-BUILT
RJH 7/6/13
STATE | PROJECT DESIGNATION | YEAR | SHEET NO. | TOTAL SHEETS
ALASKA | NH-071-3(12) / 76727 | 2009 | 43 | 50
U:\Hwy\62342\Drafting\escp\62342P01-ESCP 4 OF 11
U.S.A. BLM
CABIN
LAKE ELEVATION~2071.4'
EXISTING HIGHWAY
ROW
24"x85' CSP 1133+84
24"x139' CSP 1144+34
"O" 1136+85.39 P.C.
"O" 1140+87.50 P.T.
OBLITERATE
MATCH 1120+00 LINE
MATCH 1150+00 LINE
POND
"O" 1121+38.17 P.T.
SECTION 7
SECTION 18
36"x118' CSP 1130+24
36"x88' CSP 1135+88
36"x66' CSP 1143+36
151
36"x103' CSP 1158+12
USS 8637
LOT 1
MATCH 1150+00 LINE
MATCH 1180+00 LINE
"O" 1152+76.53 P.C.
"O" 1159+98.68 P.T.
ROCK CHECK DAMS @ 1165+00 TO 1186+00
24"x98' CSP 1178+46
24"x80' CSP 1179+45

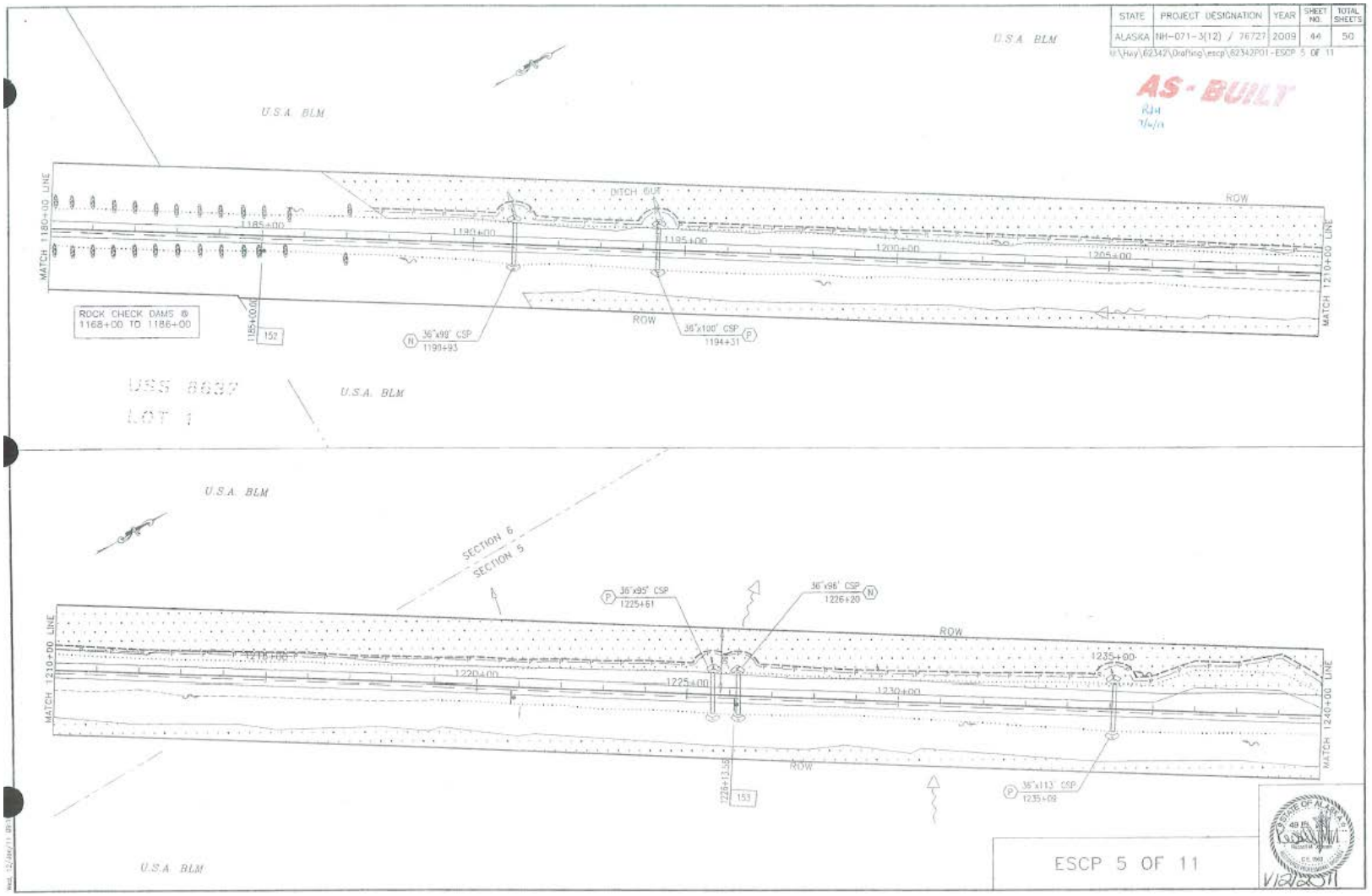
STATE | PROJECT DESIGNATION | YEAR | SHEET NO. | TOTAL SHEETS
ALASKA | NH-071-3(12) / 76727 | 2009 | 44 | 50
U:\Hwy\62342\Drafting\escp\62342P01-ESCP 5 OF 11
AS - BUILT
RJH
7/6/11
U.S.A. BLM
U.S.A. BLM
MATCH 1180+00 LINE
1185+00
1190+00
1195+00
1200+00
1205+00
DITCH OUT
ROW
ROW
MATCH 1210+00 LINE
ROCK CHECK DAMS @
1168+00 TO 1186+00
1185+00.00
152
36"x99' CSP
1190+93
36"x100' CSP
1194+31
USS 8697
LOT 1
U.S.A. BLM
U.S.A. BLM
SECTION 6
SECTION 5
36"x95' CSP
1225+61
36"x98' CSP
1226+20
MATCH 1210+00 LINE
1215+00
1220+00
1225+00
1230+00
1235+00
ROW
ROW
MATCH 1240+00 LINE
1226+13.35
153
36"x113' CSP
1235+09
U.S.A. BLM
ESCP 5 OF 11

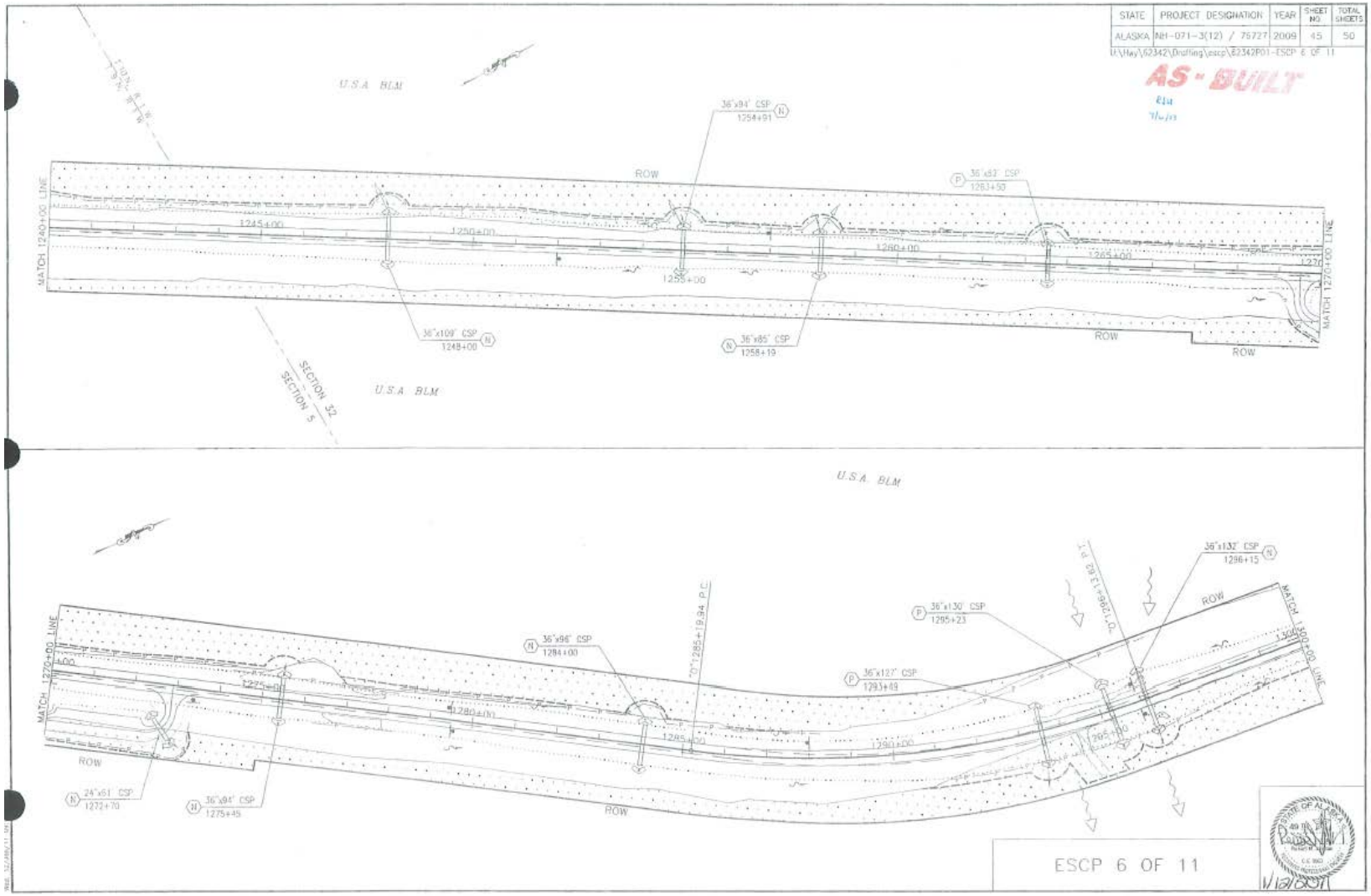
STATE | PROJECT DESIGNATION | YEAR | SHEET NO. | TOTAL SHEETS
ALASKA | NH-071-3(12) / 76727 | 2009 | 45 | 50
H:\Hwy\62342\Drafting\escp\62342P01-ESCP 6 OF 11
AS-BUILT
U.S.A. BLM
36"x94' CSP
1254+91
ROW
36"x83' CSP
1283+50
MATCH 1240+00 LINE
1245+00
1250+00
1255+00
1260+00
1265+00
MATCH 1270+00 LINE
36"x109' CSP
1248+00
36"x85' CSP
1258+19
ROW
ROW
SECTION 32
SECTION 5
U.S.A. BLM
U.S.A. BLM
36"x132' CSP
1296+15
P.T. 1286+13.80
36"x130' CSP
1295+23
ROW
MATCH 1300+00 LINE
36"x96' CSP
1284+00
P.I. 1285+19.94
36"x127' CSP
1293+49
MATCH 1270+00 LINE
1275+00
1280+00
1285+00
1290+00
1295+00
ROW
24"x61' CSP
1272+70
36"x94' CSP
1275+45
ROW
ESCP 6 OF 11

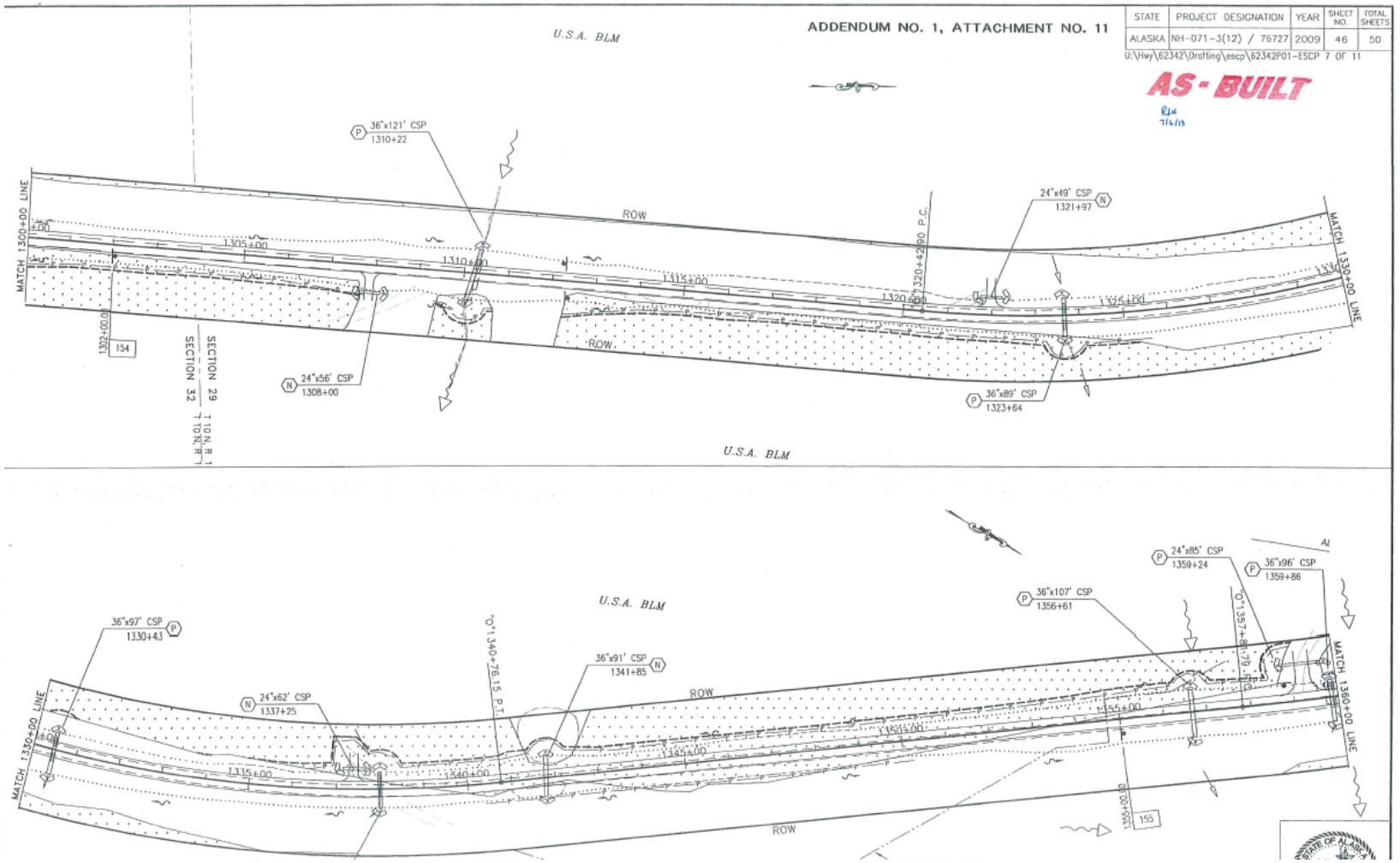
ADDENDUM NO. 1, ATTACHMENT NO. 11
STATE | PROJECT DESIGNATION | YEAR | SHEET NO. | TOTAL SHEETS
ALASKA | NH-071-3(12) / 76727 | 2009 | 46 | 50
U:\Hwy\62342\Drafting\escp\62342P01-ESCP 7 OF 11
AS-BUILT
U.S.A. BLM
36"x121' CSP
1310+22
24"x49' CSP
1321+97
24"x56' CSP
1308+00
36"x89' CSP
1323+64
ROW
MATCH 1300+00 LINE
MATCH 1330+00 LINE
SECTION 32 T10N, R1
SECTION 29 T10N, R1
154
U.S.A. BLM
36"x97' CSP
1330+43
24"x62' CSP
1337+25
36"x91' CSP
1341+85
"O" 1340+76.15 P.I.
36"x107' CSP
1356+61
24"x85' CSP
1359+24
36"x96' CSP
1359+86
"O" 1357+81.79 P.I.
MATCH 1360+00 LINE
155
ROW

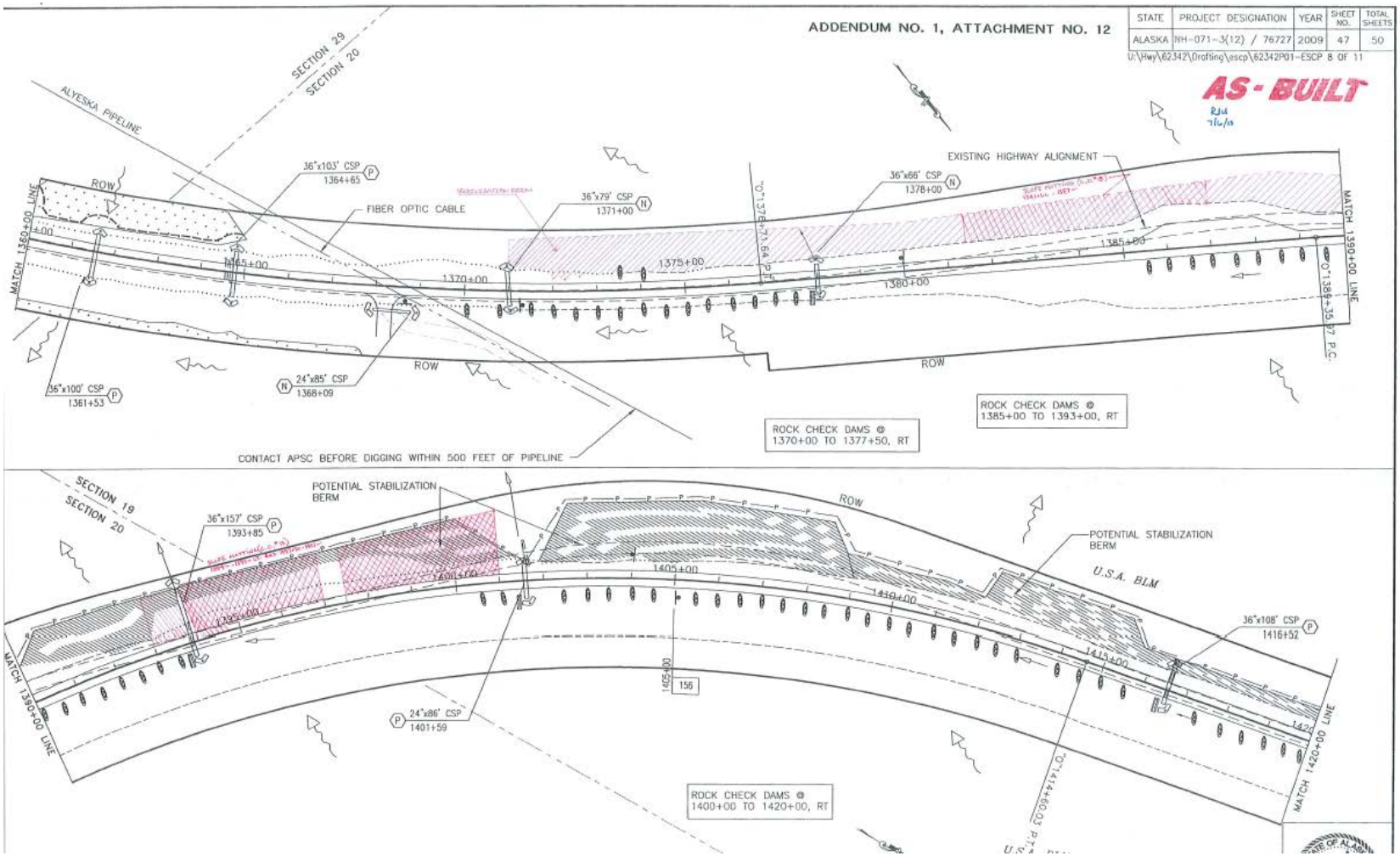
ADDENDUM NO. 1, ATTACHMENT NO. 12
STATE | PROJECT DESIGNATION | YEAR | SHEET NO. | TOTAL SHEETS
ALASKA | NH-071-3(12) / 76727 | 2009 | 47 | 50
U:\Hwy\62342\Drafting\escp\62342P01-ESCP 8 OF 11
AS-BUILT
SECTION 29
SECTION 20
ALYESKA PIPELINE
ROW
36"x103' CSP
1364+65
FIBER OPTIC CABLE
36"x79' CSP
1371+00
36"x66' CSP
1378+00
EXISTING HIGHWAY ALIGNMENT
MATCH 1360+00 LINE
MATCH 1390+00 LINE
1365+00
1370+00
1375+00
1380+00
1385+00
36"x100' CSP
1361+53
24"x85' CSP
1368+09
CONTACT APSC BEFORE DIGGING WITHIN 500 FEET OF PIPELINE
ROCK CHECK DAMS @
1370+00 TO 1377+50, RT
ROCK CHECK DAMS @
1385+00 TO 1393+00, RT
SECTION 19
SECTION 20
POTENTIAL STABILIZATION BERM
36"x157' CSP
1393+85
1395+00
1400+00
1405+00
1410+00
1415+00
U.S.A. BLM
36"x108' CSP
1416+52
24"x86' CSP
1401+59
156
MATCH 1390+00 LINE
MATCH 1420+00 LINE
ROCK CHECK DAMS @
1400+00 TO 1420+00, RT

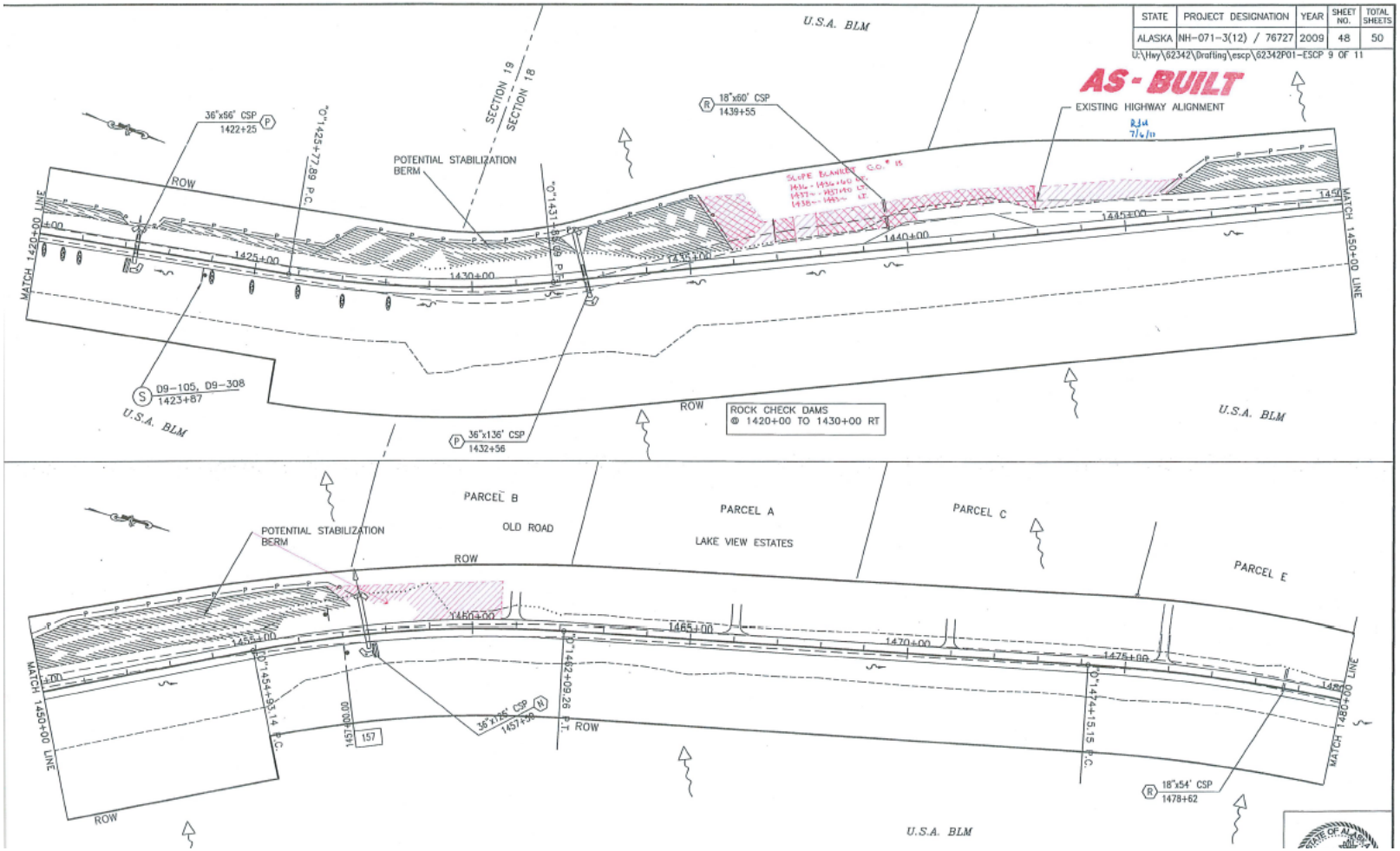


| STATE | PROJECT DESIGNATION | YEAR | SHEET NO. | TOTAL SHEETS |
|---|---|---|---|---|
| ALASKA | NH-071-3(12) / 76727 | 2009 | 48 | 50 |

U:\Hwy\62342\Drafting\escp\62342P01-ESCP 9 OF 11

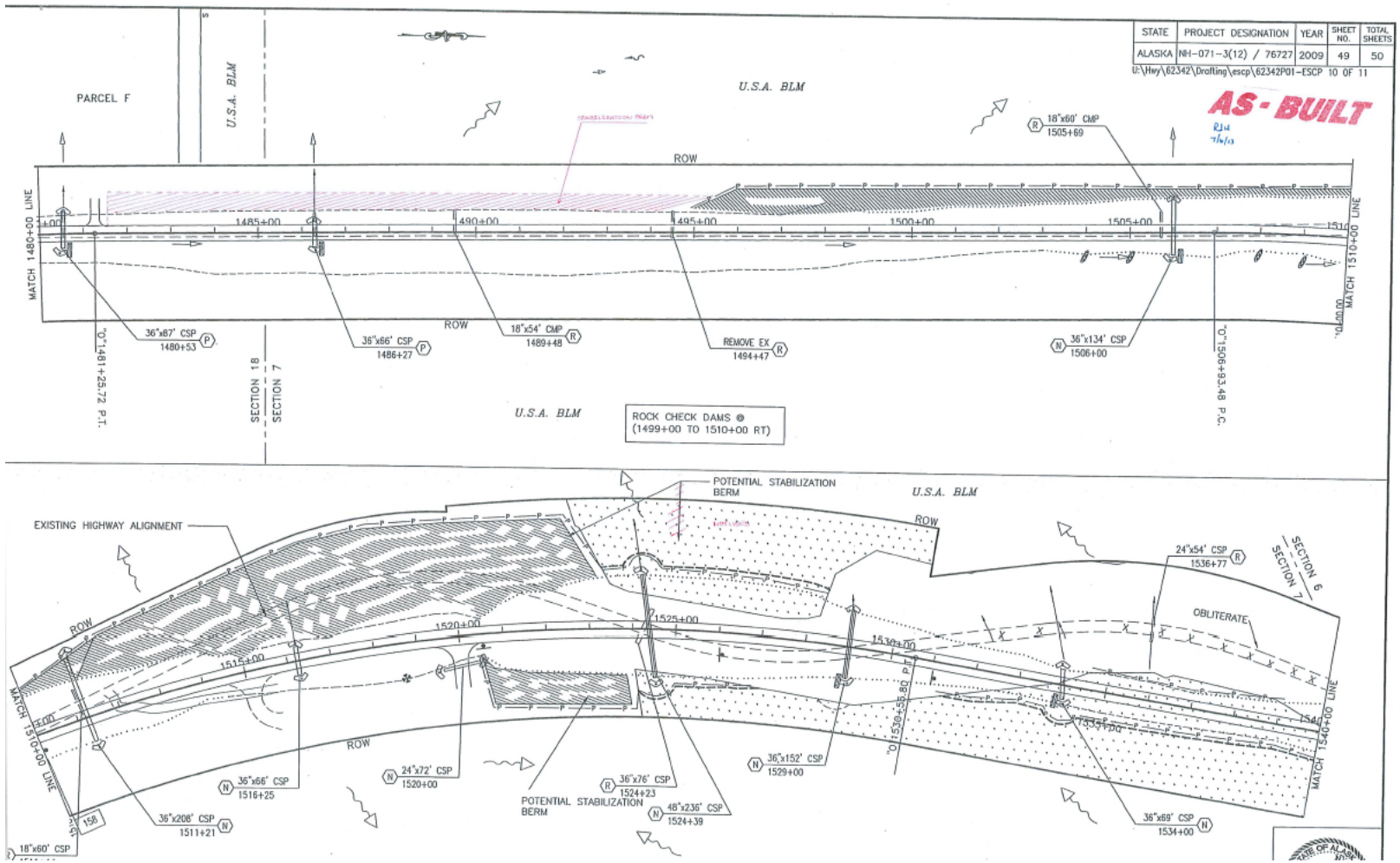
STATE
PROJECT DESIGNATION
YEAR
SHEET NO.
TOTAL SHEETS
ALASKA
NH-071-3(12) / 76727
2009
49
50
U:\Hwy\62342\Drafting\escp\62342P01-ESCP 10 OF 11
AS-BUILT
PARCEL F
U.S.A. BLM
ROW
MATCH 1480+00 LINE
MATCH 1510+00 LINE
18"x60' CMP 1505+69
36"x87' CSP 1480+53
36"x66' CSP 1486+27
18"x54' CMP 1489+48
REMOVE EX 1494+47
36"x134' CSP 1506+00
"O" 1481+25.72 P.T.
"O" 1506+93.48 P.C.
SECTION 18
SECTION 7
ROCK CHECK DAMS @ (1499+00 TO 1510+00 RT)
POTENTIAL STABILIZATION BERM
EXISTING HIGHWAY ALIGNMENT
24"x54' CSP 1536+77
SECTION 6
OBLITERATE
MATCH 1510+00 LINE
MATCH 1540+00 LINE
36"x66' CSP 1516+25
24"x72' CSP 1520+00
36"x76' CSP 1524+23
48"x236' CSP 1524+39
36"x152' CSP 1529+00
"O" 1530+56.80
36"x208' CSP 1511+21
36"x69' CSP 1534+00
18"x60' CSP

| STATE | PROJECT DESIGNATION | YEAR | SHEET NO. | TOTAL SHEETS |
|---|---|---|---|---|
| ALASKA | NH-071-3(12) / 76727 | 2009 | 50 | 50 |

U:\Hwy\62342\Drafting\escp\62342P01-ESCP 11 OF 11

AS-BUILT
RJW
7/5/11

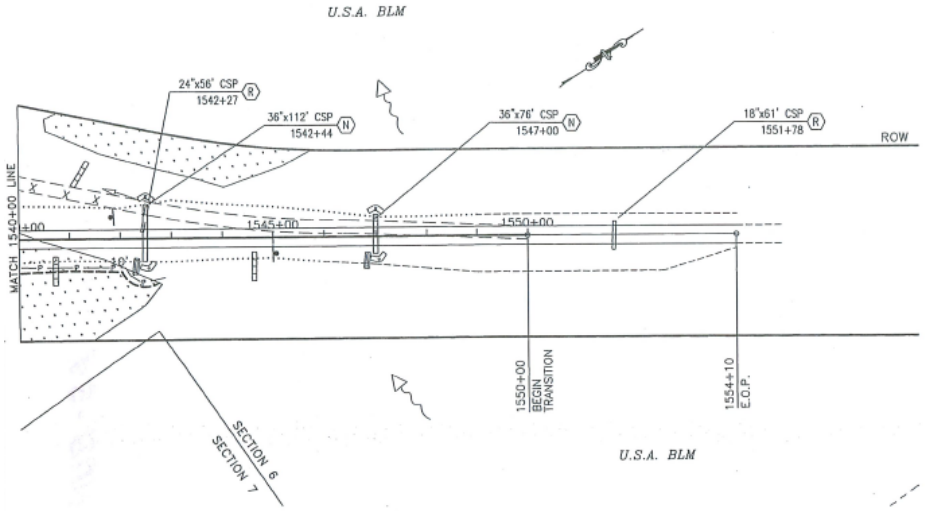

## APPENDIX C: Field Survey Results of four Sections

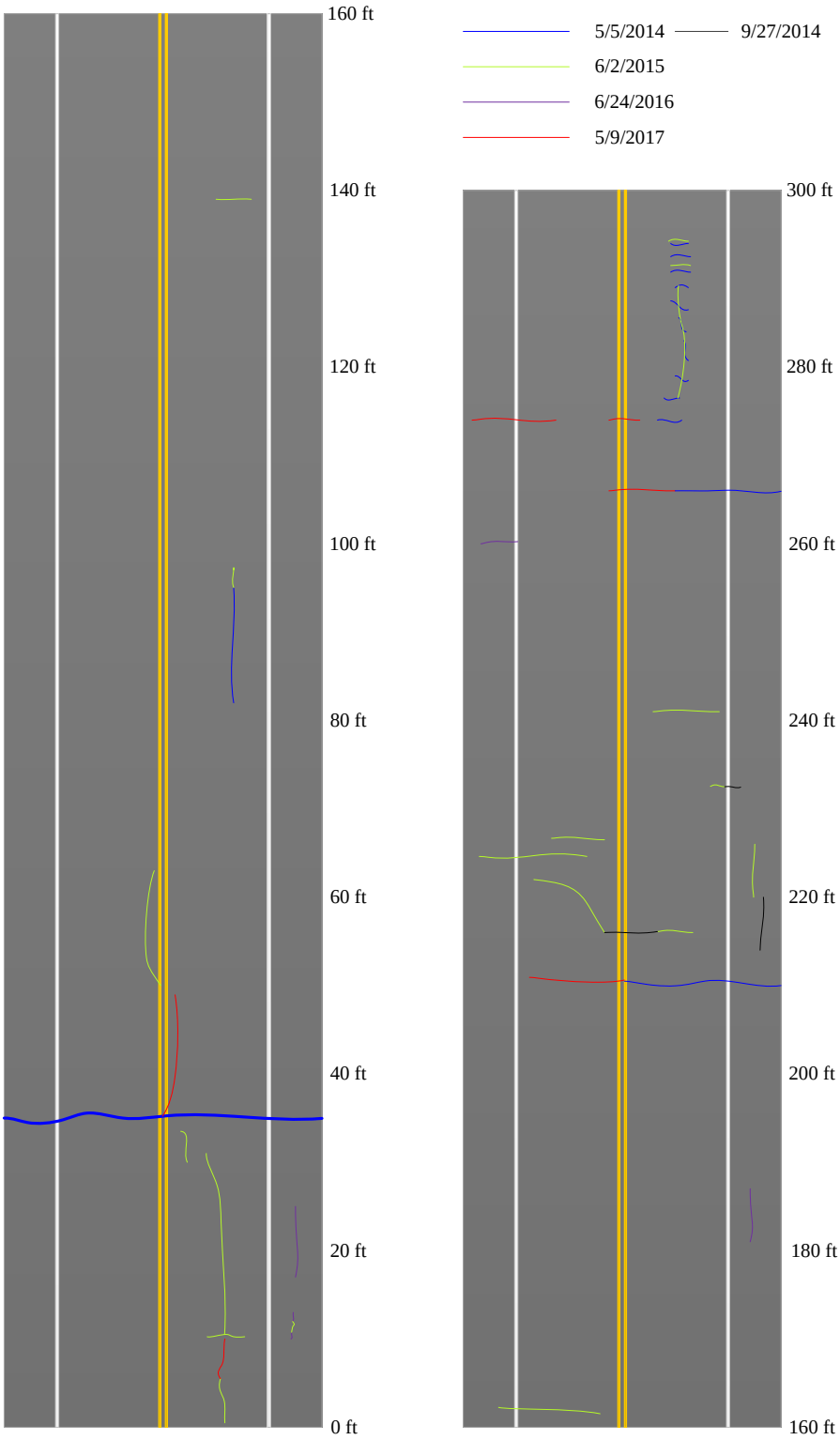


**Areas 2 and 3, G4 in the right lane**

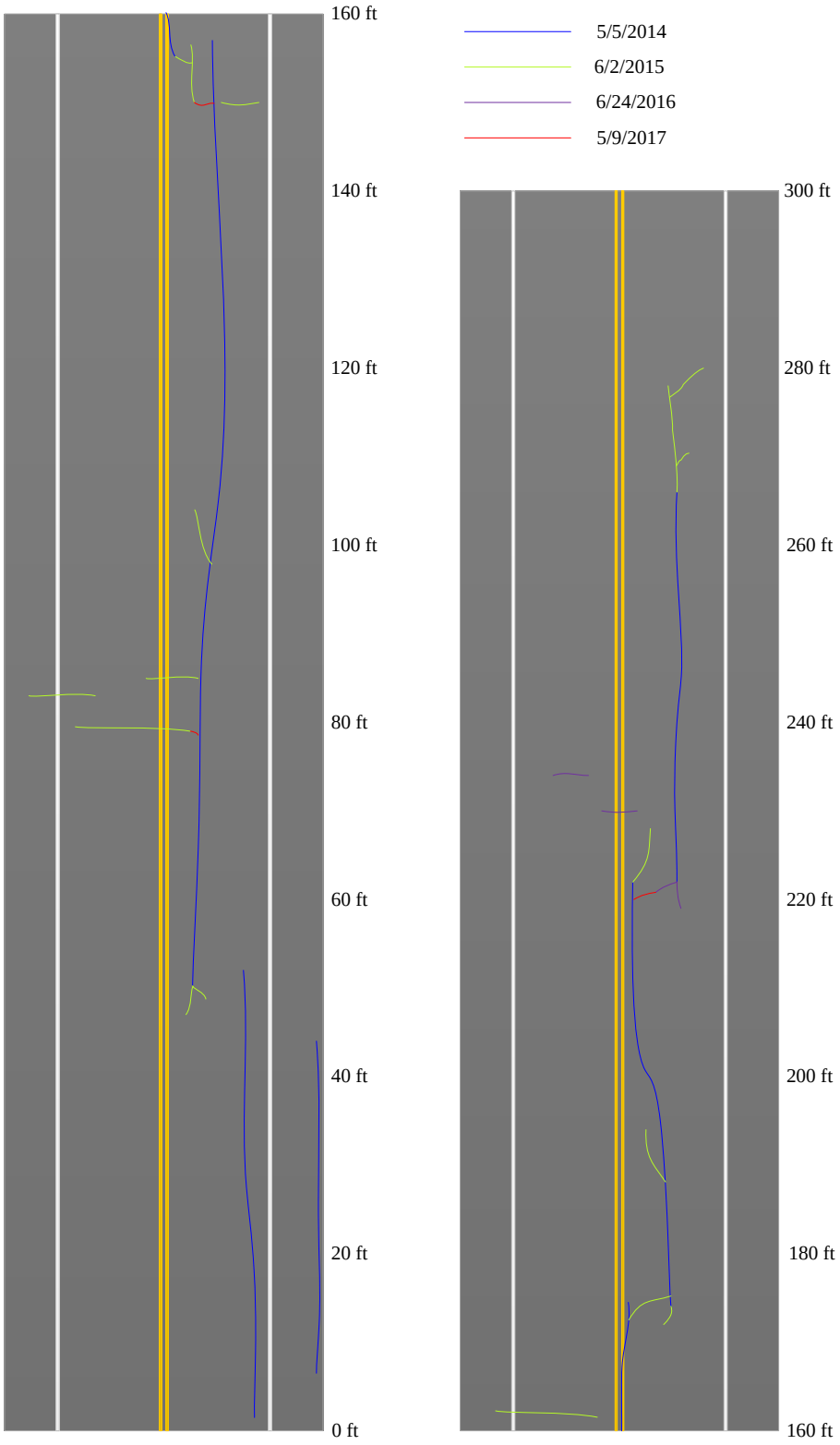


**Area 4, control section**

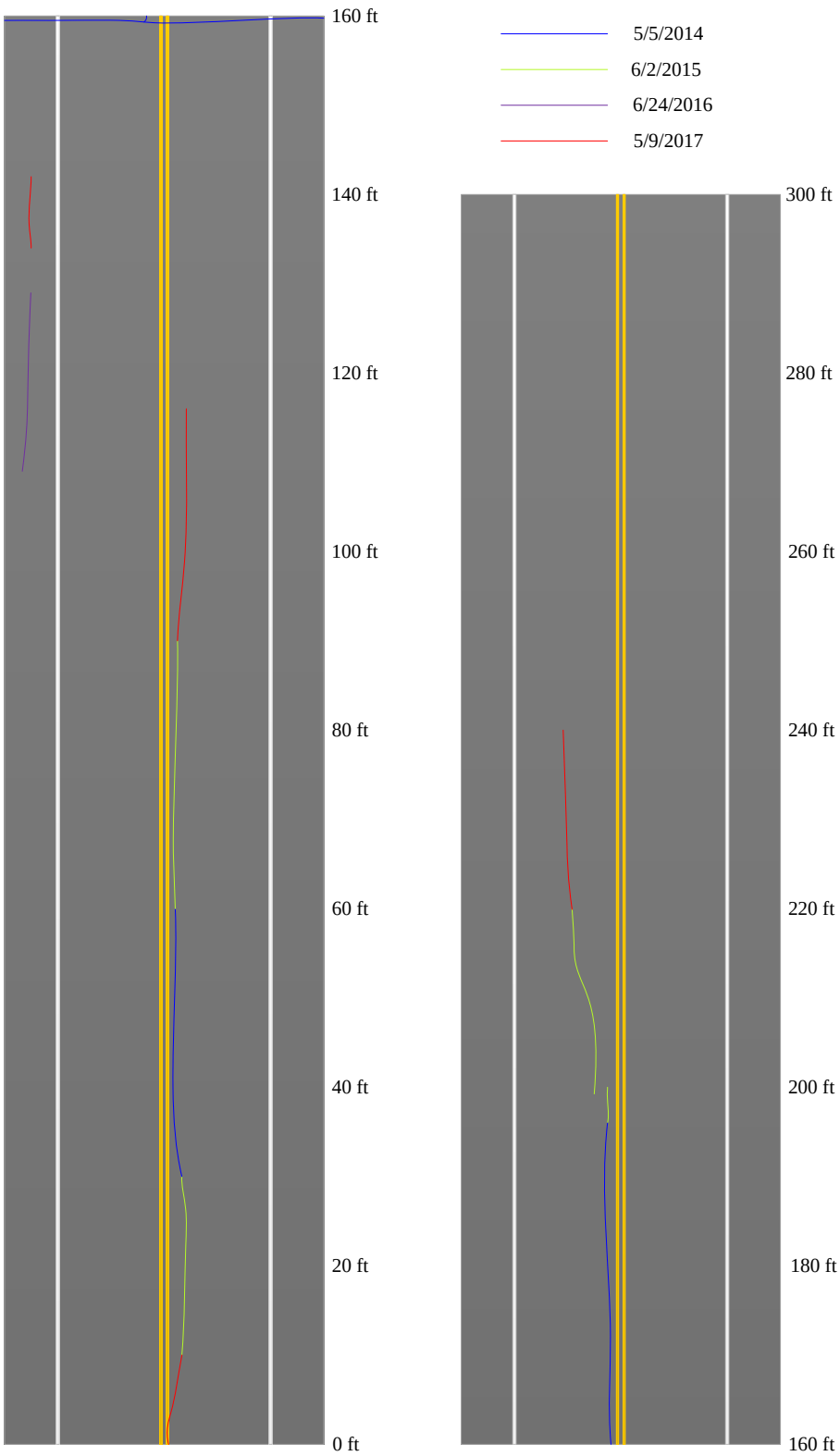


**Area 9, G50/50 in the left lane**

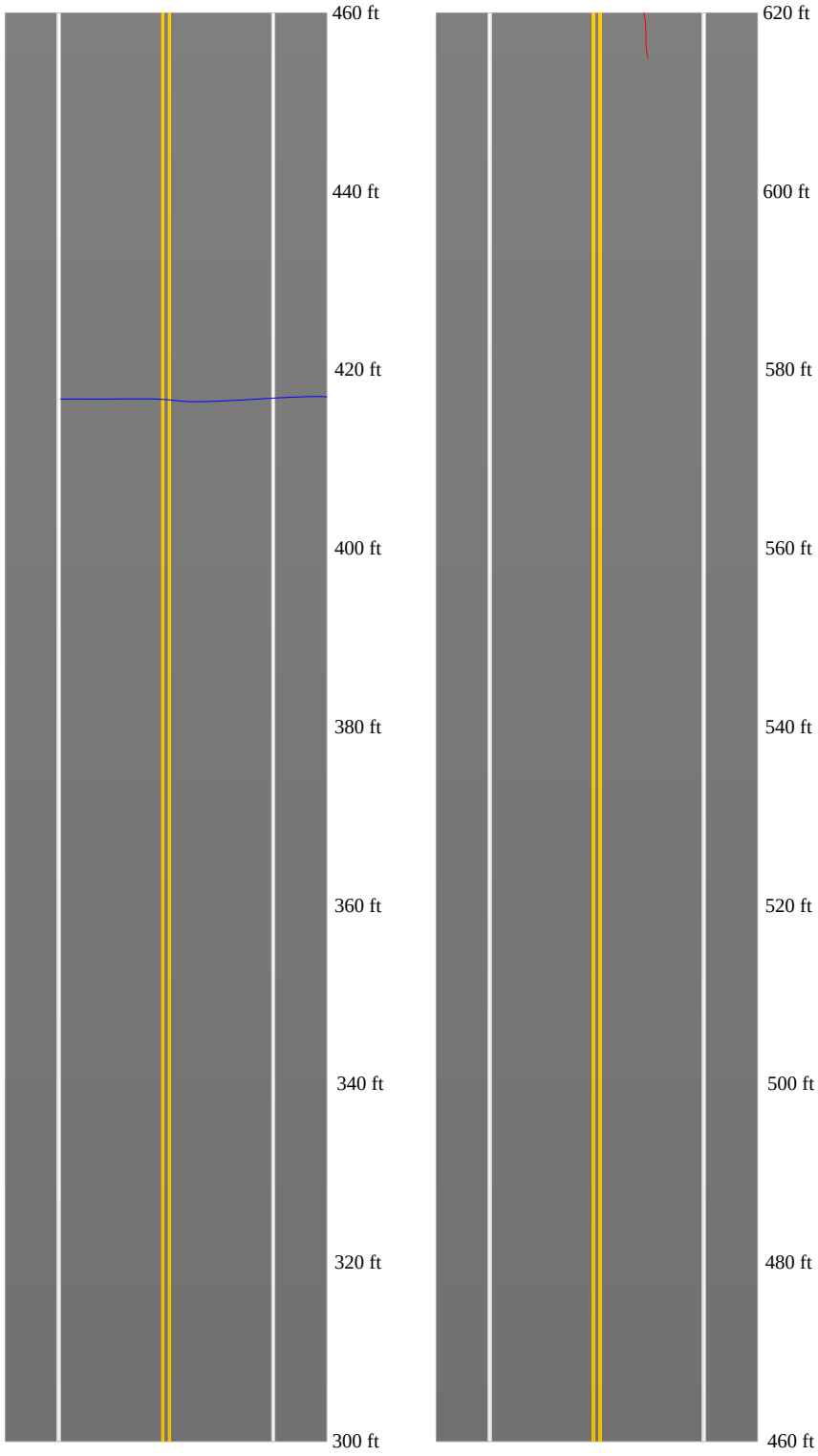


**Area 10, G100/100 in the left lane**

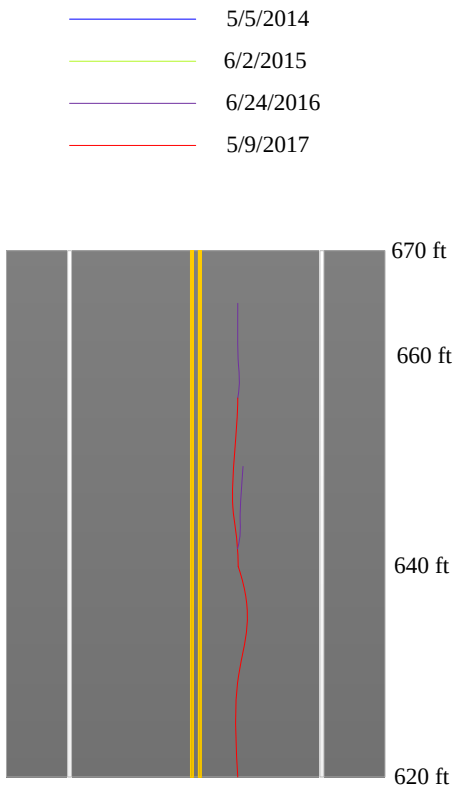


**Area 10, G100/100 in the left lane**